Mechanisms for Pd−Au enrichment in porphyry-epithermal ores of the Elatsite deposit, Bulgaria

José M. González-Jiménez[a,*], Rubén Piña[b], Thomas N. Kerestedjian[c], Fernando Gervilla[a,d], Iñigo Borrajo[e], Julia Farré-de Pablo[f], Joaquín A. Proenza[f], Fernando Tornos[e], Josep Roqué[f], Fernando Nieto[a,d]

[a] *Departamento de Mineralogía y Petrología, Facultad de Ciencias, Universidad de Granada, Avda. Fuentenueva s/n, 18002 Granada, Spain*
[b] *Departamento de Mineralogía y Petrología, Facultad de Ciencias Geológicas, Universidad Complutense de Madrid, C/ José Antonio Novais, 2, 28040 Madrid, Spain*
[c] *Geological Institute, Bulgarian Academy of Sciences, 24 Georgi Bonchev Str., 1113 Sofia, Bulgaria*
[d] *Instituto Andaluz de Ciencias de la Tierra (IACT), CSIC-UGR, Avda. de las Palmeras 4, 18100 Armilla, Granada, Spain*
[e] *Instituto de Geosciencias (IGEO, CSIC-UCM), C/Severo Ochoa, 7, 28040 Madrid, Spain*
[f] *Departament de Mineralogia, Petrologia i Geologia Aplicada, Facultat de Ciències de la Terra, Universitat de Barcelona, 08028 Barcelona, Spain*

ARTICLE INFO

ABSTRACT

Porphyry Cu can contain significant concentrations of platinum-group elements (PGE: Os, Ir, Ru, Rh, Pt, Pd). In this study, we provide a comprehensive in situ analysis of noble metals (PGE, Au, Ag) for (Cu−Fe)-rich sulfides from the Elatsite, one of the world's PGE-richest porphyry Cu deposits. These data, acquired using laser ablation-inductively coupled plasma-mass spectrometry (LA-ICP-MS), indicate that Pd was concentrated in all the (Cu−Fe)-rich sulfides at ppm-levels, with higher values in pyrite (~6 ppm) formed at the latest epithermal stage (i.e., *quartz–galena–sphalerite* assemblage) than in bornite and chalcopyrite (< 5 ppm) from the hypogene *quartz–magnetite–bornite–chalcopyrite* ores. Likewise, Au is significantly more concentrated in pyrite (~5 ppm) than in the (Cu−Fe)-rich sulfides (≤ 0.08 ppm). In contrast, Ag reaches hundreds of ppm in pyrite and bornite (~240 ppm) but is in much lesser amounts in chalcopyrite (< 25 ppm). The inspection of the time-resolved spectra collected during LA-IPC-MS analyses indicates that noble metals are present in the sulfides in two forms: (1) structurally bound (i.e., solid solution) in the lattice of sulfides and, (2) as nano- to micron-sized inclusions (Pd−Te and Au). These observations are further confirmed by careful investigations of the PGE-rich (Cu−Fe)-rich sulfides by combining high-spatial resolution of field emission scanning electron microscope (FESEM) and focused ion beam and high-resolution transmission electron microscopy (FIB/HRTEM). A typical Pd-bearing mineral includes the composition $PdTe_2$ close to the ideal merenskyite but with a distinct crystallographic structure, whereas Au is mainly found as native element. Our detailed mineralogical study coupled with previous knowledge on noble-metal inclusions in the studied ores reveals that noble metal enrichment in the Elatsite porphyry ores was mainly precipitated from droplets of Au-Pd-Ag telluride melt (s) entrained in the high-temperature hydrothermal fluid. These telluride melts could separate at the time of fluid unmixing from the silicate magma or already be present in the latter either derived from deep-seated crustal or mantle sources. Significant enrichment in Pd and Au (the latter correlated with As) in low-temperature pyrite is interpreted as remobilization of these noble metals from pre-existing hypogene ores during the epithermal overprinting.

1. Introduction

Porphyry-epithermal mineral systems are defined as large volumes (10 − > 100 km³) of hydrothermally altered rock centered on shallow-intruded porphyry stocks (i.e., porphyry Cu deposit sensu stricto) with a typical stockwork and disseminated mineralization that may be accompanied by skarn, carbonate-replacement, sediment-hosted, and high- and intermediate-sulfidation epithermal base and noble metal mineralization (Sillitoe, 2010; Lee and Tang, 2020). Porphyry copper deposits (PCDs) are the world's most important source of Cu, Mo and Re, and are major sources of Au and Ag; significant byproduct metals include Se, Bi, Zn and Pb (Sinclair, 2007; Sillitoe, 2010; Grabezhev, 2013).

Geochemical studies, based on the analysis of whole-rock samples

and mineral concentrates obtained by flotation during mining process, have shown that PCDs may also have an untapped potential to produce other metals as by-product (Economu-Eliopoulos and Eliopoulos, 2000; John and Taylor, 2016; Velásquez et al., 2020). As exemplified in the Elatsite alkaline Cu−Au porphyry, located in the Srednogorie zone of Bulgaria, hypogene *quartz–magnetite–bornite–chalcopyrite* ores linked to potassic alteration can contain up to 5 ppm of Pd + Pt (Petrunov et al., 1992; Tokmakchieva and Pazderov, 1995; Dragov and Petrunov, 1996; Tarkian et al., 2003; Augé et al., 2005). Appreciable amounts of these PGE (sub-ppm to 3 ppm) have been documented in early hypogene sulfides, formed at the earliest stages of alteration in PCDs in a wide range of tectonic settings (intra-oceanic island arcs, continental arcs and post–collisional) and hosted by geochemically different intrusive rocks (alkaline, calc-alkaline and K-alkaline). These include PCDs of the subtypes Cu−Au (Mutschler et al., 1985; Tarkian and Stribrny, 1999; Economu-Eliopoulos and Eliopoulos, 2000; Thompson et al., 2001; Economou-Eliopoulos, 2005; Summerlin, 2014; Eliopoulos et al., 2014; Logan and Mihalynuk, 2014; McFall et al., 2018; David and Timms, 2018), Cu-Mo-Au (Tarkian and Stribrny, 1999; Core et al., 2006; Pašava et al., 2010; Wang et al., 2014) and Cu−Mo (Cabri, 1981; Tarkian and Stribrny, 1999; Sotnikov et al., 2001; Berzina et al., 2007; Logan and Mihalynuk, 2014; Plotinskaya et al., 2018). These observations highlight that in addition to Cu, Au, Mo, Re or Ag, platinum-group elements (PGE) like Pt and Pd may be also recoverable from some PCDs.

The application of a range of techniques for mineral microanalysis —electron probe microanalysis (EPMA), scanning electron microscope (SEM), laser ablation-inductively coupled plasma-mass spectrometry (LA-ICP-MS), secondary-ion mass spectrometry (SIMS), and high-resolution transmission electron microscopy (HRTEM) — have shown that noble metals can be found in PCDs forming specific minerals or micro/nano-particles. These include sulfides [stromeyerite (AgCuS)], Au-Ag-bearing alloys [electrum (Au−Ag)], tellurides [hessite (AgTe$_2$); empressite (AgTe); sylvanite (Au,Ag)$_2$Te$_4$; petzite (Ag$_3$AuTe$_2$); sopcheite (Ag$_4$Pd$_3$Te$_4$)], selenides [naumannite (Ag$_2$Se); bohdanowiczite (AgBiSe$_2$); eucairite (AgCuSe)] and platinum-group minerals (PGM). The mineralogy of PGM also comprises tellurides [members of the solid solution merenskyite (PdTe$_2$)-moncheite (PtTe$_2$) solid solution series and kotulskite (PdTe)] as well as bismuthides [sobolevskite (PdBi); michnerite (Pd,Pt)BiTe] and arsenides [palladoarsenide (Pd$_2$As) and sperrylite (PtAs$_2$)]. The rare PGM are tiny grains (usually < 50 μm) found included or at the margins of larger BMS (chalcopyrite and bornite) grains as well as isolated in hydrothermal silicate minerals, forming the hypogene magnetite-bornite-chalcopyrite ores of PCDs of the types Cu−Au (Petrunov et al., 1992; Tokmakchieva and Pazderov, 1995; Tarkian and Koopmann, 1995; Dragov and Petrunov, 1996; Tarkian and Stribrny, 1999; Tarkian et al., 2003; Augé et al., 2005; Bogdanov et al., 2005; Eliopoulos et al., 2014; McFall et al., 2019), Cu-Mo-Au (Ann Mason in USA; Aird et al., 2019) and Cu−Mo (Mikheevskoe, Askug and Rio Blanco; Berzina et al., 2005, 2007; Plotinskaya et al., 2018; Crespo et al., 2018). In addition, PGM have been reported in the later stage porphyry-epithermal transition zone of telescoped deposits of Mount Milligan and Mikheevskoe (Lefort et al., 2011; Plotinskaya et al., 2018), highlighting that PGM can also occur in relatively cooler (< 270 °C) hydrothermal overprinting stages.

However, in PCDs noble metals are also found as solid solution in other minerals such as sulfides (e.g., pyrite, chalcopyrite, bornite, molybdenite, galena) and sulfosalts (e.g., tetrahedrite). These minerals are repositories not only for Au, Ag, Re and PGE but also for (semi)-metals like As, Sb, Te, Co, Ni and Zn, with concentrations varying in the range of sub-ppm levels to a few wt%. Pyrite is the main host for Au (Cook and Chryssoulis, 1990; Deditius et al., 2011; Reich et al., 2013; Gregory et al., 2013; Sykora et al., 2018) and it may be also host for appreciable amounts of PGE (Hanley and MacKenzie, 2009; Hanley et al., 2010; Pass, 2010; Serafimovski et al., 2013). Bornite preferentially concentrates Ag and Bi as well as Mo, Zn and Se, whereas chalcopyrite is able to dissolve appreciable values of Ge and Sn as well as In and Pd

(Pašava et al., 2010; Cook et al., 2011; Yano, 2012; Reich et al., 2013; George et al., 2018; Liu et al., 2020). These (Cu−Fe)-rich sulfides may also contain other economically interesting elements like Co, Ni, As, Sb, and Pb. Molybdenite from PCDs worldwide is particularly enriched in Re (Mcfall et al., 2019) as well as Cd, Ag, Te, Ba, Co, Se, Pb, and Bi (Aminzadeh et al., 2011; Ciobanu et al., 2013; Rathkopf et al., 2017; Plotinskaya et al., 2018), and tetrahedrite may also contain all these elements as well as tens of ppm of Pd and Ag (Pašava et al., 2010).

We focus our study on a suite of spatially and paragenetically well-constrained hypogene ores from the earliest stages of porphyry potassic alteration (i.e., *quartz–magnetite–bornite–chalcopyrite* at > 700–400 °C), and compare them with those formed during the latest epithermal overprint (i.e., *quartz–galena–sphalerite* at 240–300 °C). Our study integrates data generated by electron probe microanalysis (EPMA), scanning electron microscope (SEM), laser ablation inductively coupled plasma-mass spectrometry (LA-ICP-MS) and high-resolution transmission electron microscopy (HRTEM) on individual (Cu−Fe)-rich sulfides from the Elatsite Cu−Au deposit, Bulgaria. We provide new constraints on the role of PGM, bornite, chalcopyrite and pyrite as scavengers of noble metals in the Elatsite deposit. This improved understanding is used to provide insights on sources and mechanisms of enrichment of the valuable metals in porphyry-epithermal systems, highlighting the possible implications for other deposits of this style worldwide.

2. Samples and analytical methods

Six representative samples from the Elatsite mine were employed in this study, including five corresponding to the hypogene early assemblage of *magnetite–bornite–chalcopyrite* and one (sample E-36) of the porphyry-epithermal transition assemblage *quartz–galena–sphalerite* (Strashimirov et al., 2002; Tarkian et al., 2003; Georgiev, 2008). The samples belonged to Prof. Petrunov's collection and are counterparts of those previously documented in Augé et al. (2005).

Polished thin-sections of the ore-bearing samples were first studied under the optical microscope in reflected and transmitted light in an effort to characterize the minerals forming the characteristic assemblage and detect discrete minerals of the noble metals (e.g., PGM). The sulfides and PGM were imaged and identified qualitatively by their characteristic Energy Dispersive Spectra (EDS) using a Leo Gemini Field Emission Scanning Electron Microscope (FE-SEM) belonging to the *Centro de Instrumentación Científica* of the Universidad de Granada, Spain. The instrument was equipped with SE, BSE and EDS detectors. Accelerating voltage was 20 kV and beam current optimized for a sufficient number of counts for each EDS analysis. The major element compositions of base metal sulfides and PGM were then analyzed, using two electron probe microanalyzer (EPMA): (1) CAMECA SX 100 at *Centro de Instrumentación Científica* of the Universidad de Granada, Spain, and (2) JEOL JXA-9800 M at Centro Nacional de Microscopía Electrónica of the University Complutense de Madrid, Spain. Analyses were carried out using an accelerating voltage of 20 kv, a beam current of 50 nA, and a beam diameter of 1 to 5 μm. The X-ray lines analyzed were As$L\alpha$, S$K\alpha$, Ni$K\alpha$, Cu$K\alpha$, Co$K\alpha$, Zn$K\alpha$, Ag$K\alpha$, Au$K\alpha$, Sb$K\alpha$, Pb$K\alpha$, Bi$M\alpha$, Te$L\alpha$, Os$L\alpha$, Ir$L\alpha$, Ru$L\alpha$, Rh$L\alpha$, Pt$L\alpha$, Pd$L\beta$. The software applies the peak-overlap correction method.

Analyses of trace elements by laser ablation inductively coupled plasma-mass spectrometry (LA-ICP-MS) were perfomed at LabMaTer, Université du Quebec à Chicoutimi (UQAC), Canada, using an Excimer 193 nm Resolution M-50 laser ablation system equipped with a double volume cell S-155 and coupled with an Agilent 7900 mass spectrometer. Samples and reference materials were placed in the chamber together, and the reference materials were run before and after each sample. The spectra were collected for 30 s with the laser switched off to determine the base line. Then, line scans across the surface of selected grains were made using a laser beam size of 33 μm, a laser frequency of 15 Hz, a fluence of 3 J/cm^2, and a speed of lateral laser displacement of 10 μm/s. Line scans were preferred instead of spots to

observe possible variations in the trace elements across the entire grain and to have a higher representativity of the element abundances. An argon-helium gas mix was used as carrier gas. The ablated material was then analyzed using the mass spectrometer in time resolution mode using mass jumping and a dwell time of 10 ms/peak. The following isotopes were monitored: ^{29}Si, ^{34}S, ^{55}Mn, ^{57}Fe, ^{59}Co, ^{60}Ni, ^{65}Cu, ^{66}Zn, ^{69}Ga, ^{75}As, ^{77}Se, ^{95}Mo, ^{99}Ru, ^{100}Ru, ^{101}Ru, ^{103}Rh, ^{105}Pd, ^{106}Pd, ^{107}Ag, ^{108}Pd, ^{111}Cd, ^{115}In, ^{118}Sn, ^{121}Sb, ^{125}Te, ^{189}Os, ^{193}Ir, ^{195}Pt, ^{197}Au, ^{206}Pb, and ^{209}Bi. The purpose of monitoring Si, Ti and Mn was to ensure that no silicates or oxides were included in the analyses. Data reduction was carried out the Iolite package for Igor Pro software (Paton et al., 2011). Internal standardization was based on ^{57}Fe using the iron values in each individual analyzed sulfide grain determined by electron microprobe.

For the calibration of PGE and Au, we use the certified reference material Po727, which is a synthetic FeS dopped with approximately 40 ppm of each PGE and Au, provided by the Memorial University of Newfoundland. For the rest of elements, we use the certified reference material MASS-1, which is a ZnCuFeS pressed powder pellet, doped with 50–70 ppm of most chalcophile elements and provided by the USGS. The calibrations were monitored using GSE-1 g, which is a natural basaltic glass fused and doped with most elements at 300–500 ppm provided by USGS, and UQAC-FeS1, which is an in-house FeS reference material doped with trace amounts of most chalcophile elements. Analyses of these materials agreed with the certified and working values (Table 1).

Polyatomic interferences of ^{63}Cu^{40}Ar and ^{65}Cu^{40}Ar on ^{103}Rh and ^{105}Pd, respectively, were considered in the analyses on Cu sulfide minerals, i.e., bornite and chalcopyrite. This correction was not necessary in pyrite because pyrite contains very little Cu (< 0.1 wt%). ^{103}Rh resulted to be below the detection limit, so no correction was necessary. ^{106}Pd was registered in bornite and chalcopyrite instead of ^{105}Pd to avoid the Cu argide interference. ^{106}Pd was corrected for any ^{106}Cd or ^{66}Zn^{40}Ar interference by monitoring ^{111}Cd and ^{66}Zn. Detection limits for laser analyses of the sulfide minerals were calculated using background counts for the gas blank and each sulfides.

An electron transparent thin-foil sample was prepared and extracted from a selected PGM by using a Focused Ion Beam Scanning Electron Microscope (FIB-SEM) in the *Laboratorio de Microscopías Avanzadas* (LMA) at the *Instituto de Nanociencia de Aragón* (INA) – University of Zaragoza, Spain. The TEM thin foil preparation was performed using a Dual Beam FEI Thermo-Fisher Scientific, model Helios 650. The selected regions of interest containing inclusions were first covered by a thin strip (~300 nm) of C by focused electron beam induced deposition (FEBID) and subsequently with a second strip (~1 μm) of Pt. These strips act as a protection during the milling, polishing and the extraction process of the thin foils. The bulk material was first removed on both sides of the lamella by a rough Ga$^+$ ion milling with a 30 k V current at 2.5 nA and the subsequent polishing with a 30 kV current at 0.23 nA. The final polishing step was performed on the sample's inclusions until the electron transparency was achieved. This was completed by subsequently milling the thin foil with a 5 kV current at 68 pA. The electron transparency was monitored by an Everhart-Thornley SE detector and using a 5 kV electron beam. After achieving the electron transparency, the thin-foil was rapidly polished using a low energy 5 kV current at 10 pA to reduce the amorphization until a final thin foil thickness of ~90 nm was attained. Afterward it was undercut with a 30 kV at 2.5 nA current and lifted-out and transferred from the sample to a TEM grid using OmniProbe nanomanipulator with a tungsten tip. To weld the thin-foil to the tungsten tip and the TEM grid an ion-beam assisted Pt deposition was performed.

A FEI Titan G2 transmission electron microscope (TEM) equipped with Field Emission gun XFEG was used to analyse the thin-foil at the *Centro de Instrumentación Científica* of the University of Granada, Spain. This microscope that includes a spherical correction for the objective lens is equipped with 4 energy dispersive analyses of X-rays (EDX) detectors (FEI microanalysis Super X) and high-angle annular dark field

detector (HAADF). It was running for the specific analysis carried out here at 300 kV working conditions while high magnification electron microscopy images (HMEM) and High-Resolution Transmission Electron Images (HRTEM) were acquired using Gatan CCD Camera. Selected mineral areas of interest sampled within the thin-foil were the imaged and chemically characterized using a combination of EDX elemental maps HAADF (to obtain Z high contrast images) and HMEM (to characterize the texture of the grains) and HRTEM (to properly define the ordering of the mineral aggregates). All these images were treated using the Digital Micrograph® software in its Version 1.71.38 while maps were processed with the INCA® Microanalysis Suite version 4.09 software package.

## 3. Geology and ore mineralization of the Elatsite deposit

3.1. The Apuseni-Banat-Timok-Srednogorie Magmatic and Metallogenic Belt

The Elatsite porphyry Cu−Au deposit is located in western Bulgaria, about 55–50 km east of Sofia and 6–15 km south of the town of Etropole (Fig. 1a). Geologically, it belongs to the Srednogorie zone, which is a roughly east-west trending tectonic zone located between the Balkan Zone to the north and the Rhodope Massif and the Sakar-Strandja zone to the south (Fig. 1a). The Srednogorie zone is the Bulgarian segment of the Apuseni-Banat-Timok-Srednogorie magmatic belt (hereafter ABTS belt; Popov et al., 2000a), a tectonic unit of the Alpine–Balkan–Carpathian–Dynaride orogenic system (Nebauer et al., 2001; Heinrich and Neubauer, 2002). This orogen resulted from the convergence between African, Arabian and Indian plates and their collision with Eurasia that promoted the closure of the Tethys since 100 Ma ago (Schmidt et al., 2008; Handy et al., 2014). A rift-related mechanism has been proposed to explain the predominant calc-alkaline to shoshonitic magmatism of the ABTS belt (Popov et al., 2000a), although most authors better agree with a subduction scenario involving the north to northeast subduction of the African Plate below the Eurasian plate from Late Jurassic to Paleogene (see Handy et al., 2014 for review). This convergence produced the nowadays arc-like structure of ABTS belt, which extends approximately 1000 km long and 30–120 km wide. It has a N-S orientation in Romania and Serbia, and an E-W oriented belt in Bulgaria. The arc has been interpreted as either intra-oceanic magmatic arc (von Quadt et al., 2005; Kamenov et al., 2007) or an Andean-type (Richards, 2015) setting. The evolution of the ABTS belt is linked to the Vardar paleo-ocean and the subsequent collision processes during the Late Jurassic to Early Cretaceous (Popov et al., 2003). The uplift, predominating during the end of Turonian, was followed by a period of rifting during the Senonian, which was associated to the post-collisional collapse of the orogen. The latter tectonic stage was characterized by subsidence in an extensional regime that promoted the diapiric emplacement of a large, sheet-like, intrusion of primitive melts as well as the formation of horsts and grabbens controlled by transcurrent oblique faults (Chambefort and Moritz, 2006).

The central part of the Srednogorie zone is characterized by the presence of abundant types of copper mineralization, always related to calc-alkaline, sub-volcanic and volcanic rocks of Late Cretaceous age. Major deposits are found in the Panagyurishte ore district, which comprises part of the Central Srednogorie and Stara planina mountains between the towns of Pazardzhik and Etropole. They include porphyry Cu deposits (Elatsite, Karlievo, Medet, Assarel, Krassen, Petelovo, Tsar Assen and Vlaikov Vruh; Fig. 1b) related to the apical parts of subvolcanic to hypoabyssal intrusions, and locally by the underlying volcanic and crystalline basement (Bogdanov, 1986; Strashimiriov et al., 2002; von Quadt et al., 2002; Popov et al., 2000b; Tarkian et al., 2003) and their linked high-sulfidation epithermal Cu−Au deposits hosted by volcanic and subsidiary sedimentary rocks (Chelopech, Vozdol gold-polymetallic mineralization; Fig. 1b; Petrunov, 1995; Popov and Kovachev, 1996; Popov and Popov, 1997). All the aforementioned

Table 1
Reference materials and values used to calibrate the laser and corrections applied for sulfides.

Element		Co	Ni	Cu	Zn	Ga	As	Se	Mo	Ru	Rh	Pd	Ag	Cd	In	Sn	Sb	Te	Os	Ir	Pt	Au	Pb	Bi
Isotope		^{59}Co	^{60}Ni	^{65}Cu	^{66}Zn	^{69}Ga	^{75}As	^{77}Se	^{95}Mo	^{101}Ru	^{103}Rh	^{105}Pd	^{107}Ag	^{111}Cd	^{115}In	^{118}Sn	^{121}Sb	^{125}Te	^{189}Os	^{193}Ir	^{195}Pt	^{197}Au	^{206}Pb	^{209}Bi
Using Laflamme Po-727	Working value (ppm)									36.5	41.6	43.4							46.7	48	35.5	45.8		
MASS-1	Working value (ppm)																			46.20	51.90	47.00		
	Mean (ppm) n = 4																			63.52	55.43	51.00		
	Standard derivation																			1.07	1.43	2.95		
	RSD (%)																			1.37	1.07	1.09		
UQAC-FeS1	Working value (ppm)									70.60	65.00	58.70							82.50	63.50	50.00	65.00		
	Mean (ppm) n = 4									65.47	60.45	44.00							82.15	54.95	47.88	63.33		
	Standard derivation									1.07	2.00	4.08							2.05	2.25	5.60	5.13		
	RSD (%)									0.93	0.93	0.75							1.00	0.87	0.96	0.97		
Using MASS-1	Working value (ppm)	67	180	134,000	210,000	64	65	53	61				67	70		55	55	21.1					80.26	66.43
UQAC-FeS1	Working value (ppm)	636.2	25,730	22,664	257.5	17.6	1055.0	330.0	66.0				165.6		9.5	184.9	87.2	149.5					90	120
	Mean (ppm) n = 4	567.1	37,540	20,797	245.5	25.9	1091.0	304.9	64.5				165.3		8.1	164.6	71.6	181.6					82.0	115.1
	Standard derivation	9.6	840	360	18.5	0.6	47.5	5.2	1.23				7.7		0.2	11.5	5.9	3.9					2.8	4.6
	RSD (%)	0.89	1.46	0.92	0.95	1.47	1.03	0.92	0.98				1.00		0.86	0.89	0.82	1.21					0.91	0.96
GSE-1 g	Working value (ppm)	380.0	143.0	380.0	460.0	490.0	260.0	20.0	390.0				200.0	160.0	370.0	280.0	450.0						378	320
	Mean (ppm) n = 4	364.1	10.0	363.0	414.6	423.4	345.7	49.0	398.3				205.7	299.6	294.6	290.9	314.9						387.63	333.35
	Standard derivation	3.2	2.5	5.3	8.0	4.9	3.6	1.9	4.7				2.5	3.1	2.9	3.8	4.3						3.03	4.5
	RSD (%)	0.96	0.07	0.96	0.90	0.86	1.33	2.45	1.02				1.03	1.87	0.80	1.04	0.70						1.03	1.04
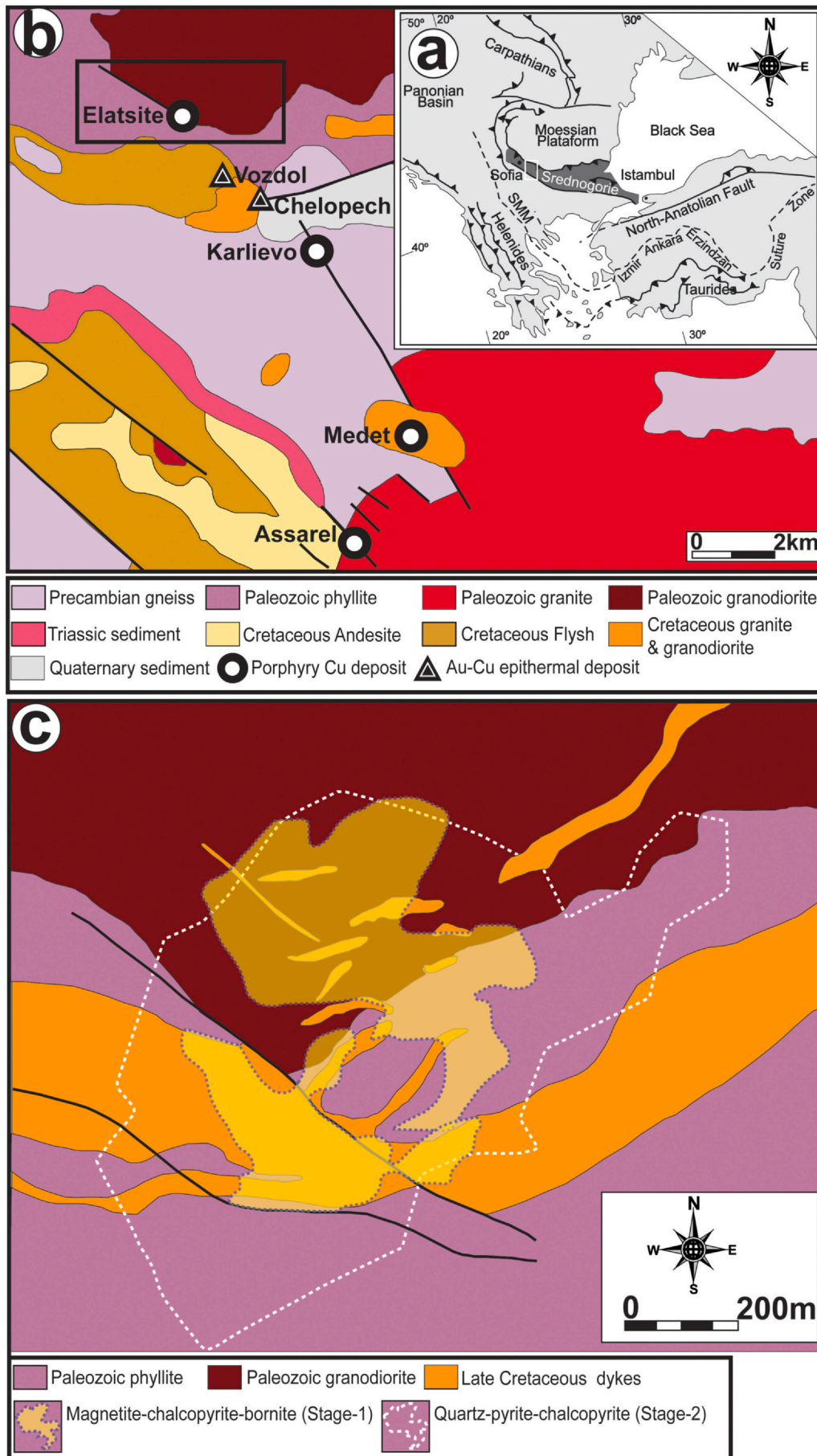
(caption on next page)

Fig. 1. (a) Geographical location of the Srednogorie zone in the tectonic frame of south-eastern Europe (after Marchev et al., 2005). (b) Geological map of the Panagyurishte district (white rectangle in a) showing the location of the Elatsite porphyry Cu−Au deposit (c). Maps shown in (b) and (c) were modified from Augé et al. (2005). Legends are in all cases inset in the figures.

deposits of the Panagyurishte district are aligned along a NW-SE lineament, which is oblique with respect to the east-west trending of the Srednogorie zone (Fig. 1a–b).

3.2. The Elatsite deposit

The Elatsite porphyry Cu−Au deposit lies about 6 km northwest of the Chelopech volcano and associated subvolcanic rocks hosting the Chelopech Au−Cu high sulfidation epithermal deposit (Fig. 1b). The mineralization was formed within the frame of the Elatsite–Chelopech volcano-intrusive complex (Bogdanov, 1987; Dimitrov, 1988; Popov et al., 2012) when dykes of granodiorite to quartz-diorite and monzodiorite intruded into the basement rocks of the Berkovitsa Group. The latter consist of Precambrian to Early Paleozoic low-grade metamorphic rocks (phyllites, quartz-sericitic schists) variably affected by contact metamorphism related to the intrusion of the Vezhen granodioritic pluton (314 ± 4.8 Ma; von Quadt et al., 2002).

The mineralization and host igneous rock are cut by NW-SE and NE-SW faults, the most significant ones being the: Elatsite fault (75–125°), Murgana fault (110–155°) and Kashana reverse slip-overthrust (~90°) (Georgiev, 2008). The mineralization is a NE-SW-trending and south dipping ellipsoidal stockwork that covers an area of 700 × 1000 m (Bogdanov et al., 2000; Popov et al., 2003). Total ore resources are estimated to be 185 million tons with 0.45% Cu, 0.3 g/t Au, 0.0046% Mo, 375 g/t Re and up to 1.9 g/t Ag.

The ore-related magmatism in Elatsite was bracketed in the time span 92.1 ± 0.3 Ma to 91.84 ± 0.31 Ma using high-precise U−Pb zircon dating on magmatic zircon, and age which is consistent with an Ar/Ar age of 91.2 ± 0.6 Ma of the hornblende, both from monzodiorite rock (von Quadt et al., 2002; Peytcheva et al., 2003; Lips et al., 2004). Additional geochronological data include molybdenite Re−Os ages at coeval 91.98 and 92.47 Ma as indicated by studies using the Re−Os isotopic system (Zimmerman et al., 2003). For a non-productive dyke of the deposit von Quadt et al. (2002) obtained a mean U−Pb zircon age of 91.42 ± 0.15 Ma.

The porphyry and host rocks show a pervasive hydrothermal alteration that includes an inner high-temperature potassic alteration that grading into a peripheral sericitic alteration, probably related to the circulation of more acid and cooler fluids (Kanazirski et al., 2002; Strashimirov et al., 2002; Georgiev, 2008). A more external zone with phyllic-argilic (Tarkian et al., 2003), argillic (Kehayov, 2005) and propylitic zones overprint the previous potassic and sericitic alteration, all of them crosscut by late, low temperature quartz-adularia-carbonate alteration (Ivanov et al., 2014).

The geochemistry, petrography and mineralogy of the Elatsite deposit and its associate ores have already been studied in detail by different authors (Hadjyiski et al., 1970; Dimitrov and Koleva, 1975; Bogdanov, 1987; Dimitrov, 1988; Petrunov et al., 1992; Tokmakchieva and Pazderov, 1995; Dragov and Petrunov, 1996; Strashimirov et al., 2002; Tarkian et al., 2003; Augé et al., 2005). Here we provide a brief summary of the main features of the mineralization according to the paragenetic sequence as provided by Popov and Georgiev (2004) and Georgiev (2008) and based on the previous classification of Strashimirov et al. (2002): Ore formation includes: (1) An early *quartz–magnetite–bornite–chalcopyrite* assemblage (Stage-1), related to the potassic alteration, which includes hydrothermal biotite, amphibole and K-feldspar with trace amounts of ilmenite and rutile. This alteration and related mineralization occur as lenses and veins penetrating the rocks of the Vezhen pluton in the north-eastern parts of the deposit (Fig. 1c). Accessory minerals also include several rare Co, Ni, Te, Bi and Se minerals as well as PGM and gold-silver alloys, selenides and

sulfides; (2) A superimposed event with a *quartz–pyrite–chalcopyrite* assemblage which is related to the phyllic alteration (Stage-2) and that makes the bulk of the economic mineralization. It consists of veinlets, pods and disseminations of sulfides that predominantly occur through the central parts of the ore bodies, replacing and enriching the Stage-1 assemblage with Cu, Au and Mo. Rare Pd-bearing minerals such as palladian rammelsbergite and palladoarsenide and Co-Ni-As minerals have been reported in this assemblage (e.g., Augé et al., 2005); and, (3) *Quartz–molybdenite* veins crosscutting Stage-1 and Stage-2 assemblages, mostly found in the central part of the deposit. An epithermal assemblage overprints this porphyry-like mineralization and consists of: (4) veins of *quartz–pyrite ± (calcite)* with small amounts of chalcopyrite, mainly found in the margins of the ore body and related to sericitic alteration. It precedes a late (5) *quartz–calcite–zeolite* assemblage with small amounts of chalcopyrite, pyrite and fluorite, and is related with the external halo of propylitic alteration. An intermediate stage between Stages 4 and 5, consisting of *quartz, galena and sphalerite*, was additionally recognized by Hadjyiski et al. (1970) in the outer south-western part of the deposit. Sphalerite and galena are the characteristic minerals of this paragenesis, although it may contain variable proportions of pyrite, chalcopyrite, and tennantite. Finally, there is local supergene alteration with precipitation of covellite and chalcocite, that it is restricted to the shallowest part of the deposit, always at depths above 50 m below the present-day topographic surface.

4. Mineralogy of the noble metals

This study focused on the *quartz–magnetite–bornite–chalcopyrite* assemblage formed in the Stage-1 of mineralization and the *quartz–galena–sphalerite* assemblage formed in some parts of the deposit between Stages 4 and 5. Consistent with previous observations, we have also identified the *quartz–magnetite–bornite–chalcopyrite* assemblage consists of magnetite, partly or totally replaced by supergene hematite, with evidence of replacement by (Cu−Fe)-rich sulfides (Fig. 2a–c; Appendix A). Frequently, bornite and chalcopyrite exhibit myrmekite-like intergrowths (Fig. 2d). Similarly, the sample corresponding to the *quartz–galena–sphalerite* assemblage, contain the typical sphalerite-dominated assemblage reported originally by Hadjyiski et al. (1970), with chalcopyrite-sphalerite overgrown by arsenic-rich pyrite partly (Fig. 2e–f).

The PGM and other minerals of the noble metals were found as isolated inclusions in, or at the margins (often in contact with amphibole) of, chalcopyrite and bornite in the sample E-18.5/1150 corresponding to the *quartz–magnetite–bornite–chalcopyrite* assemblage, formed during the Stage-1 of mineralization. These include Pd-telluride (Figs. 3a–l and 4), native gold (Fig. 3m–n) and Ag selenides (Fig. 3o–p).

4.1. Pd-telluride

Pd-telluride forms euhedral or subhedral grains of < 50 μm, located at the interface between (Cu−Fe)-rich sulfides and amphibole (Fig. 3a–d) or more commonly included within chalcopyrite or bornite (Fig. 3e–l). When in contact with the silicates, the PGM usually overgrow on (Fig. 3b), or use, them as a nucleation substrate (Fig. 3c). In situ analyses (n = 20) using EPMA show composition rather homogenous, close to the ideal stoichiometry $PdTe_2$ (Fig. 4; Appendix B). The analyzed grains contain small amounts of Pt (up to 2.64 wt%), Sb (up to 0.77 wt%), Bi (up to 0.66 wt%) and Ni (up to 0.01 wt%) (Fig. 4).

One FIB thin foil (Fig. 5a–b) was cut perpendicular to the grain boundaries between $PdTe_2$, chalcopyrite and amphibole of the grain shown in Fig. 3a–b. The cross section revealed euhedral shape of PGM and net contacts with the associated Cu-sulfide and amphibole,
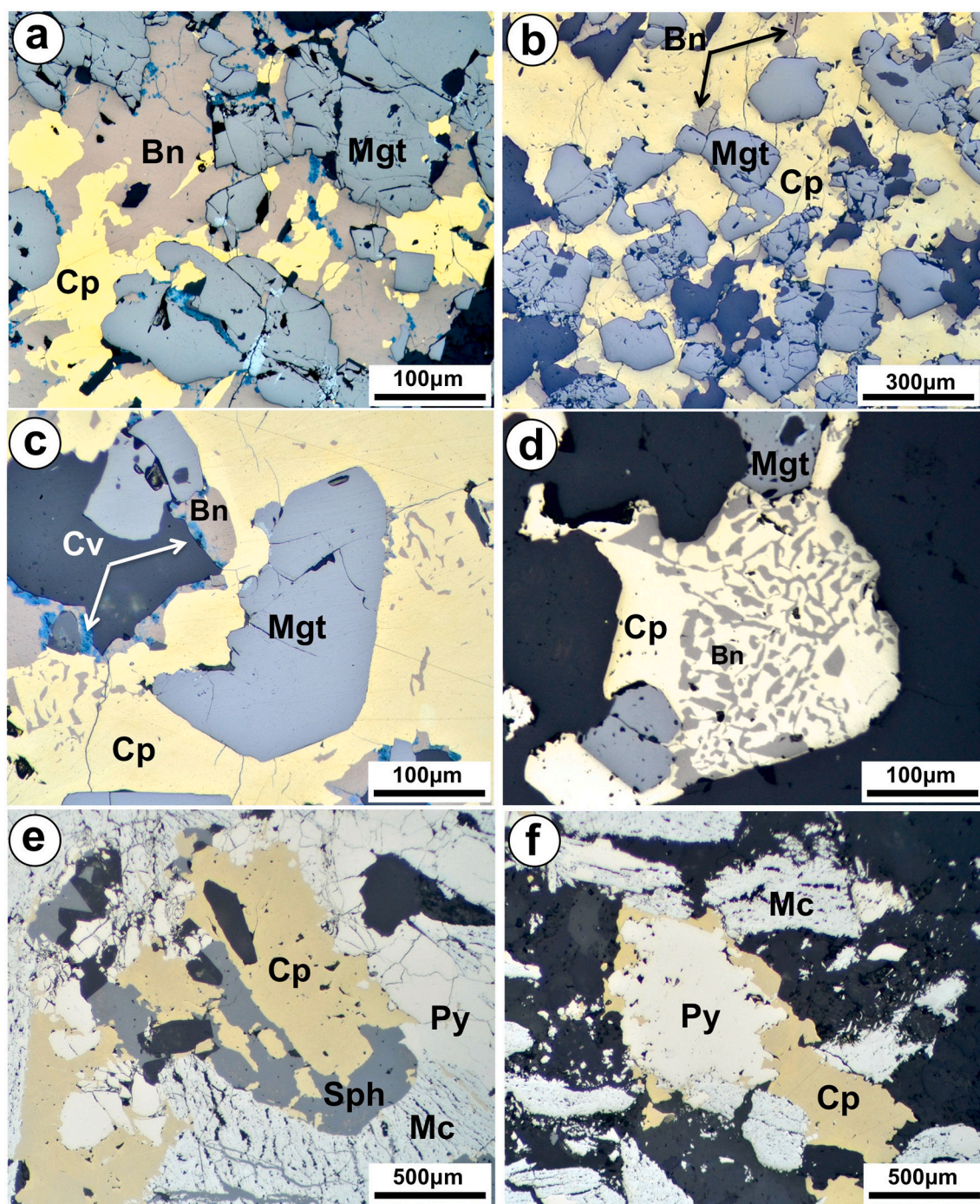
Fig. 2. Selected photomicrographs (parallel nicols under reflected light) of textural type ores from the Elatsite deposits analyzed in this study. (a–d) hypogene *quartz–magnetite–bornite–chalcopyrite* mineral assemblage (Stage-1) associated with the high-temperature potassic alteration. (e-f) epithermal *quartz–galena–sphalerite assemblage* linked formed in the transition between Stage-4 and Stage-5 of alteration.

reaching a depth of > 5 µm. The TEM-EDS elemental map of the area along the contact between the PGM and the (Cu−Fe)-rich sulfide revealed a better association between Pd and Te in the PGM grain (Fig. 5c–f). Bright-field (BF) and high-resolution (HR) TEM observations, and fast Fourier transform analyses (FFT) of the HRTEM images revealed that the PGM and the (Cu−Fe)-rich sulfide are crystalline (Fig. 6A1). High-resolution TEM images, FFT and SAED patterns obtained on selected areas through the PGM grain showed that it is a well-crystallized single crystal (Fig. 6A1, A-1A-1 and A-1A-2; Table 2). In contrast, nanostructural analysis of the host (Cu−Fe)-rich sulfides reveals a bornite-like structure underlying the surface observed on the polished thin section, instead of chalcopyrite (Fig. 6A1 and A-1B; Table 2). The HRTEM images, FFT and SAED patterns indicate that it is a mosaic-like defective orthorhombic crystal of bornite (Fig. 6A1 and A-1B). The HRTEM investigation of the grain boundary between the PGM and the (Cu−Fe)-rich sulfide and silicate show that, at the nanoscale, all these minerals have no crystallographic continuity and they are misoriented to each another (Fig. 6B1 and B2). It is worth to note that the lattice of the PGM and the (Cu−Fe)-rich sulfide are regularly arranged, which indicates that no particles of noble metals are included in these minerals. Therefore, noble metals measured in such (Cu−Fe)-rich sulfide grain hosting PGM using LA-ICP-MS are structurally bounded.
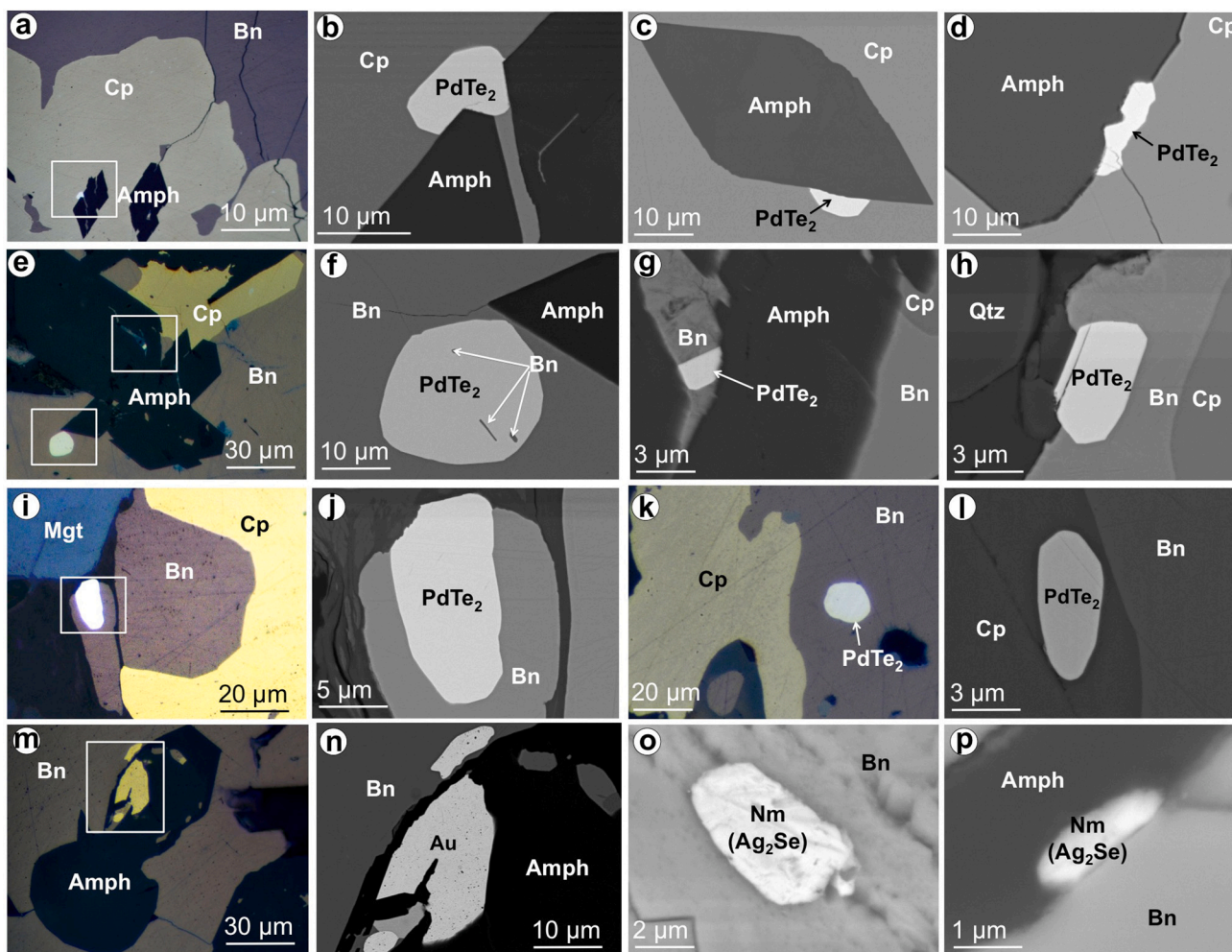
Fig. 3. Microphotographs of representative platinum-group minerals and gold identified in this study in samples containing the hypogene *quartz–magnetite–bornite–chalcopyrite* mineral assemblage (Stage-1) associated with the high-temperature potassic alteration at Elatsite. Images (a), (e), (i), (k) and (m) are microphotographs under reflected light microscope (parallel Nichols) whereas the remaining images are back-scattered images showing details of these pictures obtained by using FE-SEM. (For interpretation of the references to colour in this figure legend, the reader is referred to the web version of this article.)
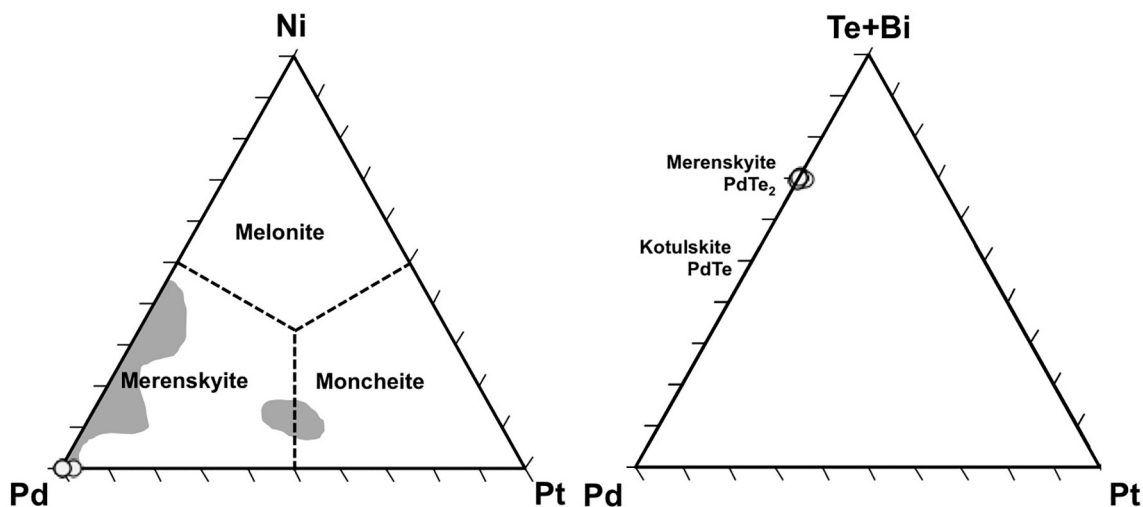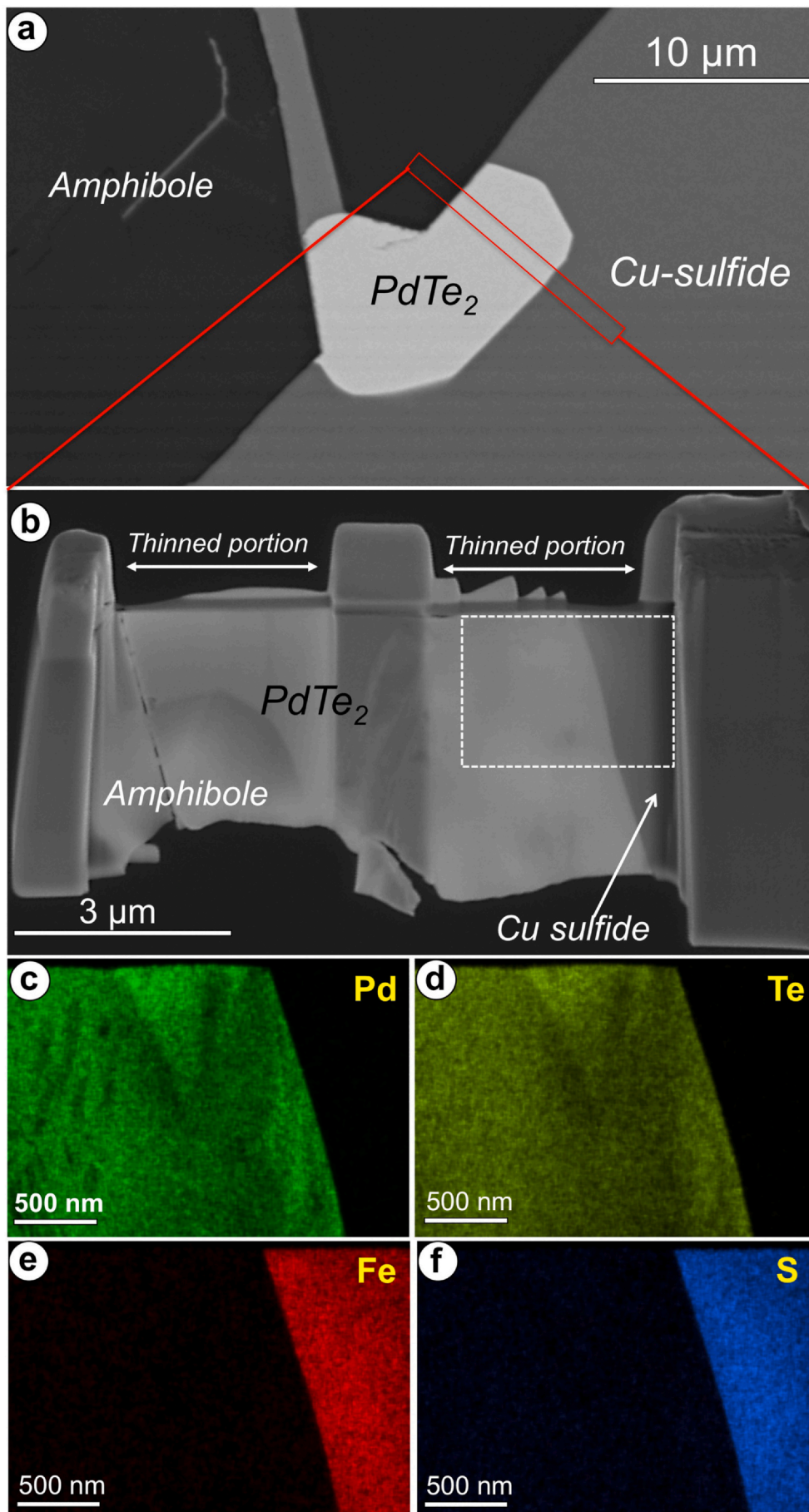

Fig. 4. Ni-Pd-Te and Te + Bi-Pd-Pt plots of the Pd-telluride grains identified in this study. Grey fields in the Ni-Pd-Te plot show compositions of the (Pd−Pt)-rich telluride reported by Augé et al. (2005) from Elatsite.

(caption on next page)

Fig. 5. (a–b) Back-scattered images of thin-foil sampled from the Elatsite PGM-bearing base-metal sulfide shown in Fig. 3a–b. (c–f) TEM-EDS elemental map acquired at the contact between the Pd-telluride and the hosting (Cu−Fe)-rich sulfide.
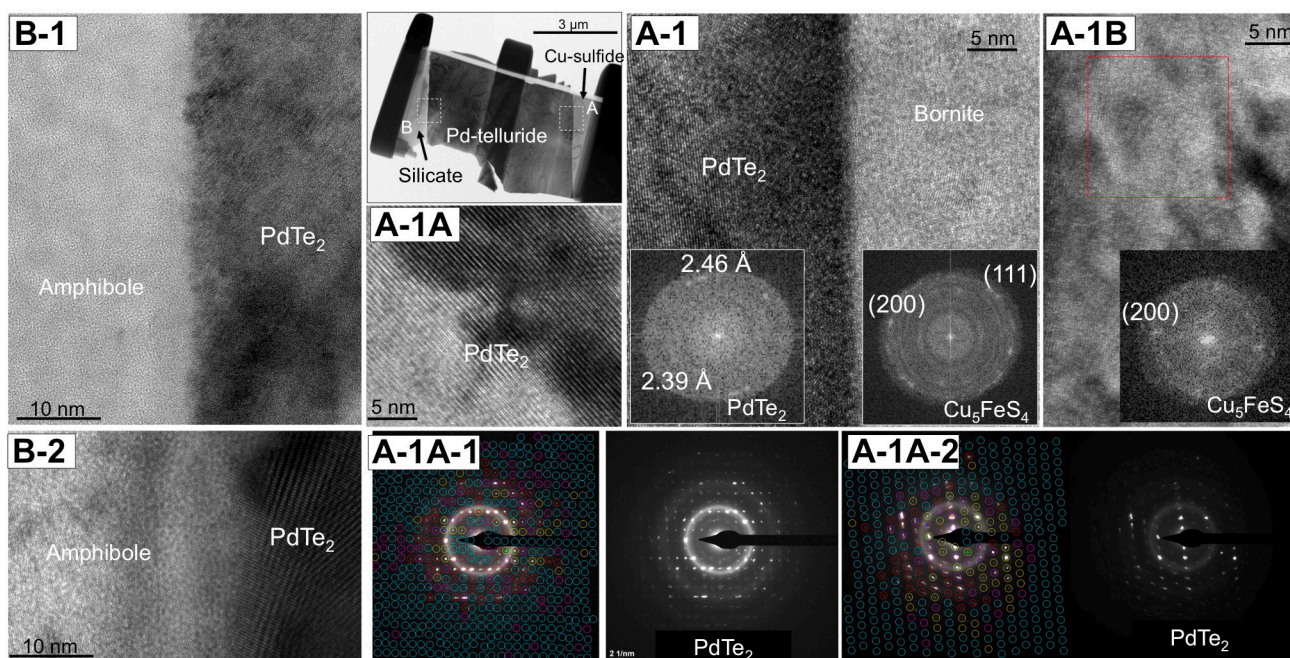

Fig. 6. Low- and high-magnification HRTEM images and associated Fast Fourier Transform (FFT) of HR image and SAED of the Pd-telluride and the hosting (Cu−Fe)-rich sulfide and amphibole of the thin foil shown in Fig. 5. Note that image A-1A-1 and A-1A-2 show the matrix of points selected for measured d-spacing from the acquired SAED that are provided in Table 2.

Table 2
Indexed SAED and FFT d-spacing values for Pd-telluride and bornite shown in Fig. 6.

(hkl)	Pd-telluride measured FFT d-spacing	Pd-telluride measured SAED d-spacing	Merenskyite PdTe$_2$ (hexagonal) theoretical d-spacing[a]	Bornite measured FFT d-spacing	Bornite (orthorhombic) theoretical d-spacing
002	2.46	2.55			
002	2.39	2.55			
001		7.29	5.11		
		4.07			
100		3.65	3.48		
		3.64			
101		2.79	2.87		
		2.14			
102		2.04	2.06		
111				3.95	4.06[b]
200				2.74	2.74
220				1.92	1.93

Reference d-spacing of merenskyite (PdTe$_2$) from Matkovic and Schubert (1978).

Reference d-spacing for bornite (Cu$_5$FeS$_4$) from Koto and Morimoto (1975).

[a] We give a reference of the closest d-spaces of merenskyite for comparison to those measured here.

[b] We give a reference of 4.06, because it is a denser plane, but very close to its position there are two more plains at 3.87–202 and 240. All three planes, probably contribute for the observed FFT intensity.

4.2. Gold

Discrete grains of up to 250 μm across of native gold alloy were found at the contacts between bornite or magnetite and the silicate matrix (Fig. 3m–n). The analyses of five of these gold grains show a relatively homogenous composition in terms of Au (90.95–91.34 wt%) and Ag (7.92–8.26) as well as negligible amounts of other metals (Appendix B).

4.3. Ag selenides

Two minute (< 2 μm across) anhedral grains of Ag selenide were identified within bornite and at the contact between bornite and amphibole (Fig. 3o–p). These two grains were too small for reliable in situ EPMA analysis, although their energy-dispersive X ray (EDS) spectrum acquired by using FESEM suggest a composition close to naumannite (Ag$_2$Se) as previously documented by Augé et al. (2005) in this deposit.

4.4. Minerals detected in sulfides during LA-ICP-MS

The examination of the time-resolved spectra signals collected during LA-ICP-MS analyses of the bornite, chalcopyrite and pyrite revealed two different types of signals for the noble metals (Fig. 7a–f). As exemplified in Fig 7a, c and e most sulfides yield an almost continuous distribution in time of Pd and Au, suggesting that these metals are structurally bound (i.e., in solid solution) within the analyzed sulfides. However, some other sulfides yield signals with narrow Pd−Te peaks (e.g., bornite and chalcopyrite in Fig. 7b and d) suggesting the presence of nano-to-micron-sized inclusions of Pd-telluride similar to those observed under optical microscope and FESEM. Likewise, pyrite may also contain inclusions of Au- and Ag-bearing minerals such as illustrated by the spiky distribution of these noble metals shown in Fig. 7f as well as minute Pt-bearing inclusions (not shown).

5. In situ noble metal concentrations in Cu- and Fe-rich sulfides

In situ LA-ICP-MS analyses show that the three sulfide types analyzed in this study (bornite, chalcopyrite and pyrite) contain appreciable amounts of noble and PGE (Rh, Pd, Au, Ag) as well as base-metals (Co, Ni, Zn, Ga, Mo, Cd, In, Sn, Bi and Pb) and semi-metals (As, Se, Sb, Te) (Fig. 8; Appendices A and C).
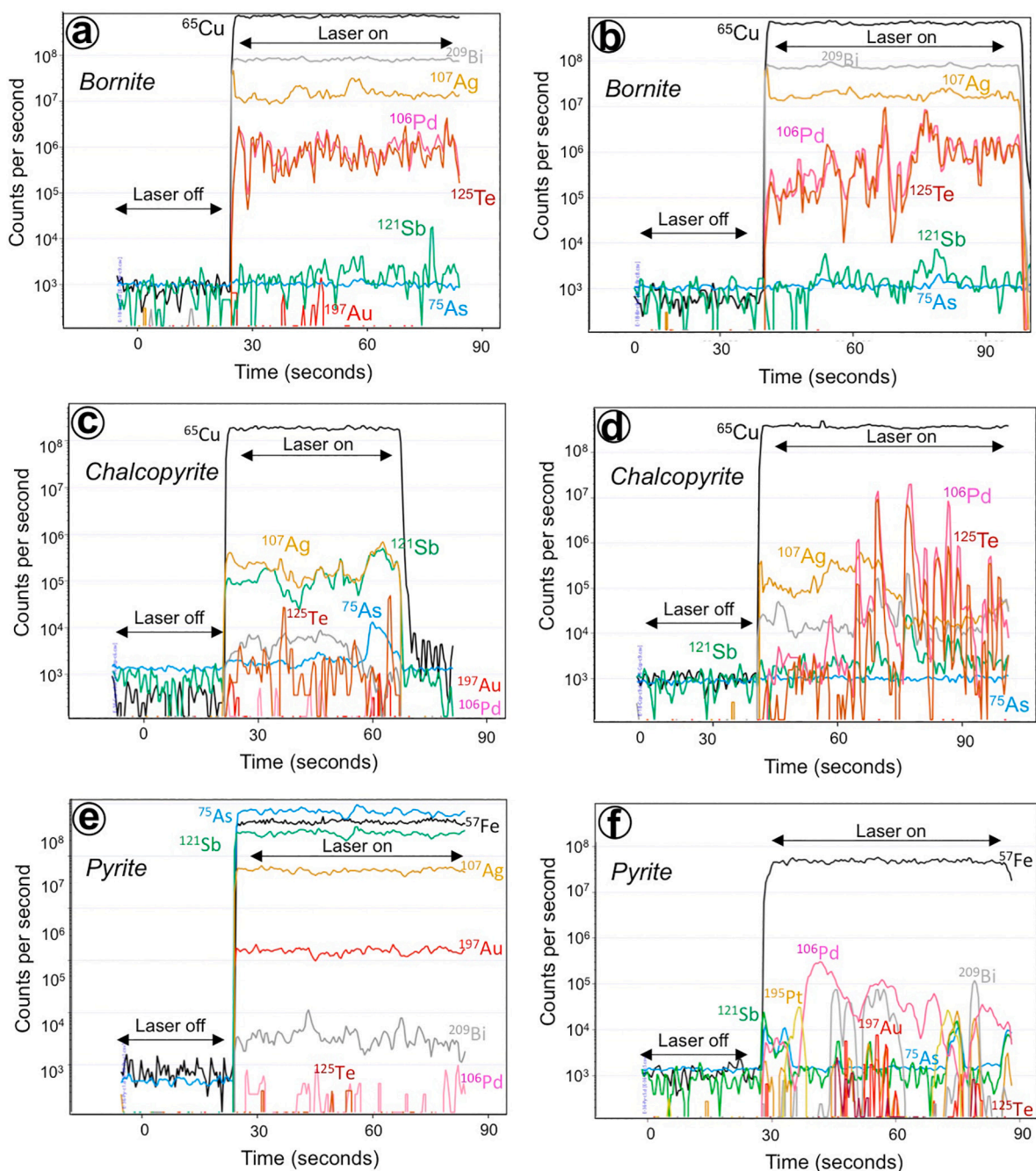
Fig. 7. Representative time-resolved LA- ICP-MS spectra collected during trace element analyses of bornite (a–b), chalcopyrite (c–d) and pyrite (e–f) at Elatsite. The transient spectra show homogenous signals for Pd, Au and Ag indicating elements in solid solution (a, c and d) whereas spikes of these elements coupled with semimetals (Te, As, Sb) in other grains (b, d, f) indicate the presence of nano-to-micron-sized particles of noble metals in these analyzed sulfides.

Noble metals (PGE + Au + Ag) are concentrated in almost identical amounts in pyrite (up to 247 ppm) and bornite (up to 221 ppm) but at a lesser extent in chalcopyrite (up to 26 ppm). Os, Ir, Ru and Re are below detection limits in all the analyzed sulfides, whereas some amounts of Rh and Pt were detected at ppb-levels in pyrite and chalcopyrite, respectively. Pd is concentrated in all the base-metal sulfides (BMS) at ppm-levels, with higher values in pyrite (up to 5.7 ppm) and bornite (up to 5.3 ppm) than in chalcopyrite (up to 3.3 ppm). Gold is mainly concentrated in pyrite (up to 5.4 ppm) but little in the (Cu−Fe)-rich sulfides (≤ 0.08 ppm), whereas Ag reaches hundreds of ppm in pyrite and bornite (~240 ppm) but is present in much lesser amounts in chalcopyrite (up to 26 ppm).

The concentrations of base-metals impurities (Pb, Cu, Ni, Co, Zn,

Ga, Mo, Cd. In, Sn) are highly variable in the analyzed BMS, ranging from few to thousands ppm. Maximum total values in pyrite are 1800 ppm whereas chalcopyrite and bornite correspond to slightly lower total amounts of these metals ~1450 ppm. Among the base-metals, Pb is the most abundant with values exceeding a thousand ppm in all the BMS. Aside Cu, Ni and Co are found in relatively high amounts in pyrite (≥ 900 ppm), but are present in much lower amount in chalcopyrite and bornite (≤ 65 ppm). Zinc, Ga, Mo, Cd, In and Sn occur in low abundances in all BMS, with maximum concentrations ranging commonly between 0.5 and 40 ppm with a few single-spot analyses reaching 150 ppm.

Relatively high amounts of As (up to 187,300 ppm) and Sb (up to 6230 ppm) are concentrated in pyrite relative to (Cu−Fe)-rich sulfides
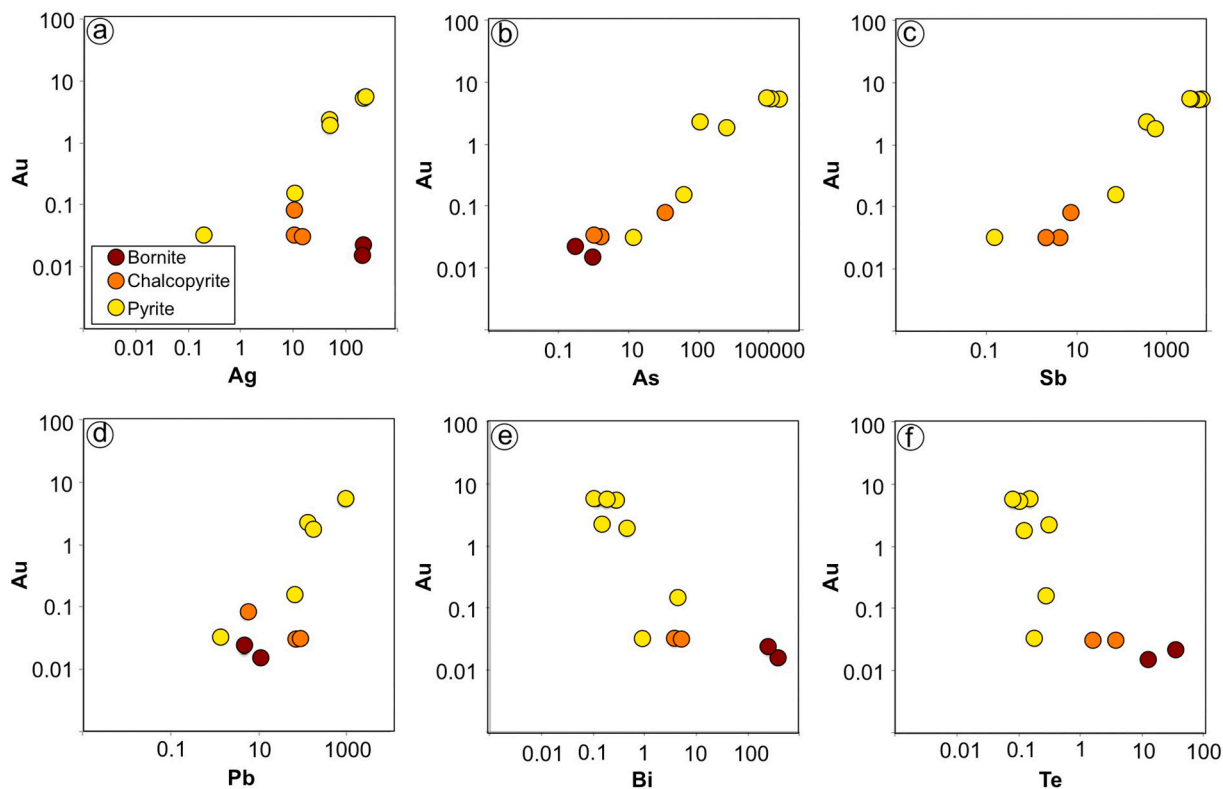
Fig. 8. Binary plots showing positive and negative correlations among representative trace elements analyzed here using LA-ICP-MS on bornite and chalcopyrite from the hypogene *quartz–magnetite–bornite–chalcopyrite* mineral assemblage (Stage-1) and pyrite from the epithermal the *quartz–galena–sphalerite* assemblage.
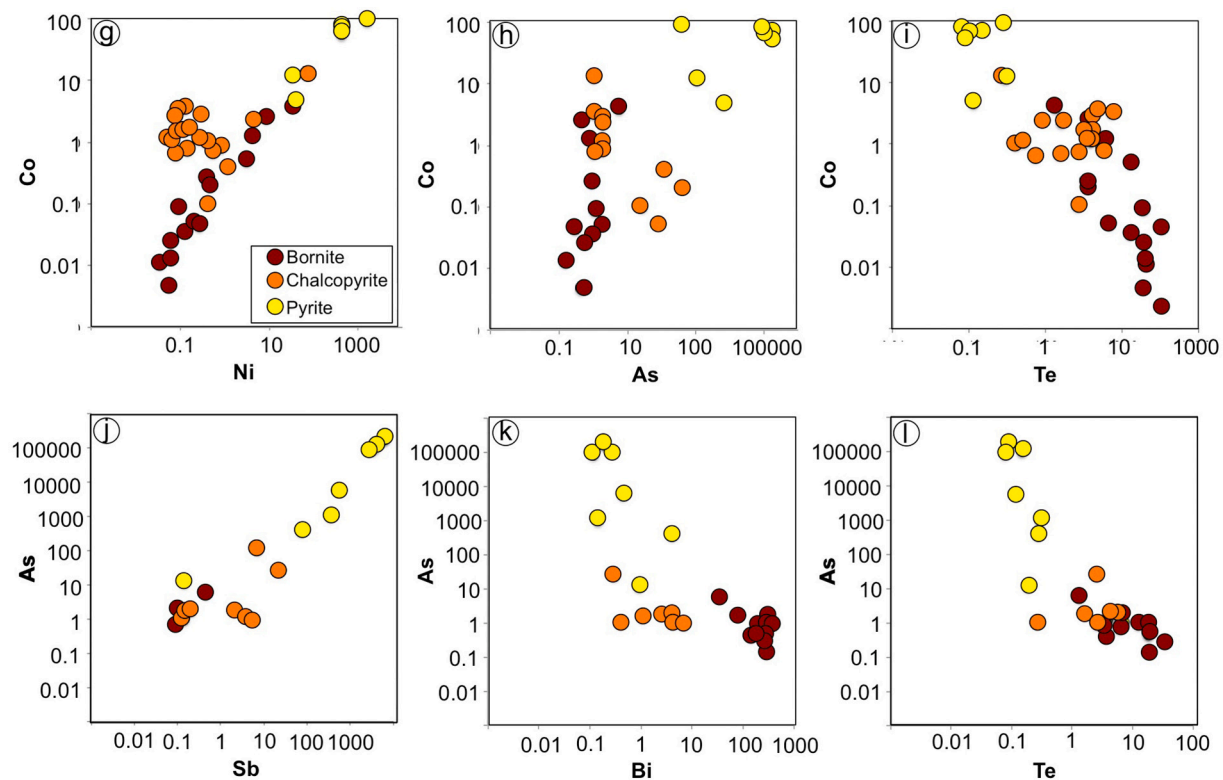

Fig. 8. (*continued*)

(commonly < 100 ppm). Selenium contents are barely similar in all sulfides, of the order of hundreds of ppm whereas Te reaches a maximum content of 33 ppm in bornite and is significantly lower in chalcopyrite (7.2 ppm) and pyrite (0.3 ppm). In addition, Bi is preferentially concentrated in bornite (up to 375 ppm) than in chalcopyrite (< 12 ppm) and pyrite (< 4.2 ppm) respectively.

No evident correlation was observed between the concentration of different PGEs, nor between PGEs and other metals. However, there is a clear correlation between Au with Ag and the semi-metals As and Sb, with progressively higher values of all these elements from bornite to chalcopyrite and pyrite, respectively (Fig. 8a–c). In contrast, Au is barely correlated positively with some of the base-metals (Co, Ni, Zn, Cd, In and Pb) (Fig. 8d), but negatively with Bi and Te (Fig. 8e–f). These correlations are particularly remarkable in the case of pyrite. Most metals (Co, Ni, Zn, Ga, Te) correlate positively with each other and with Sb and As (e.g., Co−As) (Fig. 8g–h), although negative trends have also been observed between Co and Ga with Te (Fig. 8i), or Bi with As (Fig. 8k). In addition, there are positive correlations between the semi-metals As−Sb and Se−Te (Fig. 8j), but negative between As−Se, Sb−Se, and Te with Sb and As (Fig. 8l).

6. Discussion

6.1. Genesis of Pd–Au–Ag–Te ± Se ± Bi minerals of the quartz–magnetite–bornite–chalcopyrite assemblage

The PGM grains identified in this study are all Pd-tellurides with composition close to ideal $PdTe_2$, strongly depleted in Bi and Pt (Figs. 3–4; Appendix B). They were found only forming part of the *quartz–magnetite–bornite–chalcopyrite* assemblage, formed in the porphyry Stage-1. These Pd-telluride grains systematically occur as micrometer-sized inclusions within chalcopyrite and bornite or at their margins, commonly associated with amphibole (Fig. 3a–l). They were also identified hosted in these sulfides by inspection of the time-resolved spectra obtained during LA-ICP-MS analyses of these sulfides (Fig. 7b and d). Previous authors (e.g., Tokmakchieva and Pazderov, 1995; Tarkian and Stribrny, 1999; Tarkian et al., 2003; Augé et al., 2005) interpreted PGM as exsolution products from the Cu−Fe sulfides deposited by hydrothermal fluids. The HRTEM investigation carried out here on the grain boundary between the PGM and the (Cu−Fe)-rich sulfide and silicate show that, at the nanoscale, these two minerals have no crystallographic continuity and they are misoriented according to each other (Figs. 5–6). Moreover, no gradational change in the contents of Pd and Te is noticeable in the proximities of the minerals contact (Fig. 5c–f). These observations exclude the possibility that PGM formed by a low-temperature induced exsolution mechanism of Pd and Te, initially hosted within the (Cu−Fe)-rich sulfide. Rather, the rounded, and occasionally euhedral, morphologies of the Pd-tellurides (e.g., Fig. 3c, f and k), often adapting to amphibole (Fig. 5a), suggest that PGM could represent the solid products of droplets of Pd-Te-rich melt, like those documented for similar Pd-tellurides associated with BMS in magmatic PGE-deposits (e.g., Sudbury; Dare et al., 2014).

The fact that some grains of Pd-telluride adapt their morphology to silicates, cemented by Cu-sulfides (Fig. 3a) clearly supports that droplets of Pd-Te-rich melt were already entrained in the high-temperature magmatic-hydrothermal fluid during the potassic alteration. These droplets of Pd-Te-rich melt would have been trapped by bornite and/or chalcopyrite, growing from the hydrothermal fluid, and then crystallized as the system cooled. Interestingly, McFall et al. (2018) suggested that droplets of Au-Pd-Bi-Te melt coexisted with the hydrothermal fluid that precipitated (Cu−Fe)-rich sulfides of the quartz–magnetite–bornite–chalcopyrite assemblage at the Skouries porphyry copper deposit. Their interpretation was also sustained on the basis that these PGM exhibiting rounded and droplet-like morphologies, found not only hosted in (Cu−Fe)-rich sulfides, but also within coexisting quartz. We have not identified in this study grains in quartz nor in magnetite

predating the deposition of (Cu−Fe)-rich sulfides, although some bleb-like gold grains were found fully hosted in amphibole crystallized before the (Cu−Fe)-rich sulfides (Fig. 3m).

Available experiments in the Pd−Te binary system indicate that melt exists above 489 °C for compositions of 40 at.% Pd and 60 at.% and still persist at 710 °C for compositions of 30 at.% Pd and ~70 at.% Te (close to the ideal formula $PdTe_2$) (Chattopadhyay et al., 1986; Kim and Chao, 1990). Moreover, available experimental data in the Pd–Te–Bi system (Hoffman and Maclean, 1976; Makovicky, 2002) indicate that $PdTe_2$ (merenskyite) has an upper thermal limit of 740 °C, although variations in composition of the latter may modify this temperature. Thus, in the solid-solution series merenskyite ($PdTe_2$)– moncheite ($PtTe_2$), the substitution of Pd for Pt increases the upper thermal limit of merenskyite, as moncheite can form up to 1150 °C (Cabri, 1981), whereas the substitution of Te for Bi strongly produces the opposite effect (Hoffman and Maclean, 1976). At Elatsite, the Pd-telluride grains with composition close to $PdTe_2$ are anomalously depleted in Bi (< 0.66 wt%), although rather platinum rich (up to 16.14 wt%; Tarkian et al., 2003) spanning towards the composition of moncheiite (Fig. 4; Augé et al., 2005), suggesting crystallization at ≥ 740 °C. All these temperatures overlap with the thermal range estimated for fluid inclusions trapped in quartz from the magnetite–bornite–chalcopyrite assemblage at Elatsite, estimated by Tarkian et al. (2003) at > 700–340 °C and by other authors (Bogdanov et al., 2000; Strashimiriov et al., 2002; Kehayov et al., 2003) at 600–340 °C. Consistently, pre-ore hydrothermal rock alteration in contact with the early subvolcanic-hypoabyssal igneous bodies at Elatsite is estimated to have formed at even much higher temperatures. This crystallization temperature is higher than that estimated by McFall et al. (2018) for merenskyite of the *quartz–magnetite–bornite–chalcopyrite* assemblage at Skouries (≤ 490 °C), which has much lower Pt (< 2.5 wt%) content but higher Bi (3.2 wt%).

The observation that Pd-telluride at Elatsite exhibits a composition close to the ideal stoichiometry of merenskyite ($PdTe_2$) but distinct structure to that defined for this mineral by Matkovic and Schubert (1978) is intriguing (Figs. 4 and 6; Table 2). Hoffman and MacLean (1976) reported that merenskyite $PdTe_2$ has a hexagonal sheeted-like Cd $(OH)_2$ structure whose *c* cell-unit parameter may increase with incorporation of Bi. However, the mineral analyzed here is virtually Bi-free, thus suggesting the possible existence of a low-temperature Bi-free $PdTe_2$ polymorph, which is predicted to have a lower-symmetry monoclinic (?) structure [A. Vymazalová (written. commun.)]. Nevertheless, further experimental work is necessary to confirm this hypothesis.

On the other hand, native gold shows the same textural relationship like PGM in the *quartz–magnetite–bornite–chalcopyrite* assemblage, suggesting that it also crystallized earlier than (Cu−Fe)-rich sulfides (Fig. 3m and n). Considering the model proposed above, one could expect that if Te-rich and Bi-bearing immiscible melt was present before then, or at the earliest stages of potassic alteration at Elatsite, it scavenged not only Pd, but also Au and Ag (Douglas, 2000). This is consistent with the fact that the *quartz–magnetite–bornite–chalcopyrite* assemblage at Elatsite also contains several grains of Au−Ag tellurides [sylvanite ($AuAgTe_2$), hessite (Ag_2Te), empressite (AgTe) and stüzite ($Ag_{5-x}Te_3$)] (Tarkian et al., 2003; Augé et al., 2005; Bogdanov et al., 2005). These Au−Ag tellurides display size and morphological features similar to those of the PGM and gold documented here (Bogdanov et al., 2005). Thus, they commonly form micrometer-sized composite droplet inclusions within chalcopyrite and bornite or at their margins, commonly associated with other hydrothermal alteration silicate minerals. Typical polyphase inclusions comprise sylvanite ± hessite ± stüzite ± empressite ± electrum ± Au ± Te ± $PdTe_2$. In contrast, biphasic ones include empressite +Te, sylvanite + Te or $PdTe_2$ with exsolutions or rims of hessite, but without any evidence of replacement textures (Petrunov et al., 1992; Tarkian et al., 2003; Augé et al., 2005; Bogdanov et al., 2005). The drop-like or anhedral shape of the

inclusions, and mutual curvilinear boundaries between crystallized phases within individual inclusions (e.g., Bogdanov et al., 2005) may indicate that they also crystallized from a melt, instead of being directly deposited by a hydrothermal fluid (Ciobanu et al., 2006; Oberthür and Wiser, 2008). This is consistent with the results of several experiments in ternary and binary systems with Au, Ag, Te indicating that Au-Ag-Te melts exits at > 435 °C (Markham, 1960; Cabri, 1965; Kracek et al., 1966; Tesfaye et al., 2013). This temperature overlaps the thermal range of the potassic alteration at Elatsite. Moreover, the results of experimental works indicate that hessite and electrum can coexist at > 550 °C (Markham, 1960), whereas the biphasic assemblage of sylvanite + Te is indeed stable at the temperature of condensation of native Te (~550 °C) (Kracek et al., 1966; Tesfaye et al., 2013) and $PdTe_2$ + hessite at ≤450 °C (Vymazalová et al., 2015). However, even though those droplets of immiscible Te-rich melt enriched in Pd, Au and Ag, coexisting with the hydrothermal fluid that precipitated (Cu−Fe)-rich sulfides, other telluride-bearing assemblages were not present during their formation, due to the lower thermal stability of some of the Te-rich minerals. For example, the mineral assemblages consisting of sylvanite + stützite + Te or sylvanite + stützite + hessite are stable below 330 °C (Cabri, 1965; Afifi et al., 1988) and the biphasic assemblage stützite + Te should form even at much lower temperature (< 260 °C) via the decomposition of empressite by the following reaction proposed by Afifi et al. (1988):

$$5AgTe \rightarrow Ag_{5-x}Te_3 + 2Te \qquad (1)$$

where AgTe is empressite and $Ag_{5-x}Te_3$ (x = 0.24–0.36) is stützite, or alternatively below 191 °C via the reaction suggested by Voronin et al. (2017):

$$5AgTe \rightarrow Ag_{5-x}Te_3 + 3Te \qquad (2)$$

Furthermore, the lesser abundance of Bi-bearing minerals [e.g., wittichenite (Cu_3AgBiS_3Se), bohdanowiczite ($AgBiSe_2$), kawazulite (Bi_2Te_2Se); naumannite (Ag_2Se), native Bi] accompanying the assemblage of Pd-Au-Te-rich tellurides at Elatsite (Augé et al., 2005; Bogdanov et al., 2005) distinguished it from other porphyry copper (e.g., Santo Tomas II or Skouries; Tarkian and Koopmann, 1995; McFall et al., 2018), where Bi minerals predominate. It indicates that, although present, Bi had a minor role in the metalloid-rich melt, which acted as a collector for noble metals.

6.2. Timing the formation of immiscible telluride melt

The "melt metalloid collector model" discussed above was originally proposed by Douglas (2000) as an alternative mechanism for gold deposition in low-temperature hydrothermal systems. Since then, it has been increasingly considered a key mechanism to explain noble metal enrichment not only for ores associated to porphyry-epithermal transition (e.g., Cook and Ciobanu, 2004; Guimarães et al., 2019; McFall et al., 2018), but also to other styles of mineralization of the magmatic-hydrothermal spectrum such as intrusion-related gold deposit veins (McCoy, 2000), Au skarns (Cepedal et al., 2006) and volcanic massive sulfide (VMS) deposits (Toermanen and Koski, 2005). Experimental (Douglas, 2000; Helmy et al., 2007; Tooth et al., 2008) and empirical (Farrow and Watkinson, 1992; Magyarosi et al., 2002; Ciobanu et al., 2005, 2010) results in the Au-Ag-Pd-Te-Bi-Na-Cl-S-H-O system show that Te and Bi-rich melts can form at the time of separation of an aqueous fluid from a crystallizing silicate melt or directly from the magmatic-hydrothermal fluid at any time during their cooling path. This mechanism of separation of telluride melt is related to changes of temperature and/or the redox state, affecting those chloride or poly-telluride complexes able to mobilize Te in such types of S- and CO_2-rich hydrothermal fluids (Tooth et al., 2008; Brugger et al., 2012; Smith et al., 2017). At Elatsite, the mineral assemblages consisting of Fe−Ti, Cu-Fe-Co-Ni-Te-Bi-Se-Au-Ag-Pd and Ag-Se ± Te, Bi associated with the *quartz–magnetite–bornite–chalcopyrite* assemblage of Stage-1 were

formed at very low fO_2 (below to the magnetite-hematite buffer) and fS_2 (Strashimiriov et al., 2002; Tarkian et al., 2003; Bogdanov et al., 2005; Georgiev, 2008). These are conditions suitable for the segregation of metalloid-rich melts from the hydrothermal fluid (Ciobanu and Cook, 2002) such as it attests the presence of some amounts of native Te and Bi (Tokmakchieva and Pazderov, 1995; Bogdanov et al., 2005; Georgiev, 2008). An early segregation of Te-rich melt can explain the formation of observed mineral assemblages as well as the relatively low (ppm-level or below detection limit) contents of Pd, Au and Ag in solid solution within hydrothermal chalcopyrite and bornite (see below).

An alternative/complementary scenario is that droplets of immiscible Te-rich melt(s) already existed in the parental alkali magma, and they transferred along with its inventory of noble metals to the hydrothermal fluid exsolved in the latest stages of magmatic activity of the porphyry system. The analysis of natural samples and empirical studies indicate that Te concentrates in natural magmas at much lower values than its measured solubility in silicate melts (Helmy et al., 2019). As a consequence, the segregation of telluride melts directly from high-temperature silicate melts is unlikely, unless Te is added from an external source. The analysis of several samples (> 190) collected from the primary geochemical halo of the Elatsite deposit does not support an external introduction of Te from crustal rocks (Popov and Georgiev, 2004). However, experiments in the Fe–Cu–Ni–Pd–Pt–Te–S system show that the separation of a telluride melt from an initial sulfide melt, enriched in Te is possible from ~900 °C (Helmy et al., 2007; Sinyakova et al., 2019). The immiscible separation of sulfide-telluride melts depends on the Te/S ratio, which may strongly vary during fractionation or oxidation (i.e., S-loss) of the sulfide droplets (Helmy et al., 2007; Holwell and McDonald, 2010; Holwell et al., 2019). In porphyry systems, sulfide droplets, which may be extracted from the lower and more mafic parts of the magma chambers (Halter et al., 2005; Cocker et al., 2016) as well as from deep-crustal (Core et al., 2006; Chiaradia, 2014; Hou et al., 2017; Hou and Wang, 2019) or mantle sources (Griffin et al., 2013; Holwell et al., 2019), could be dissolved at any time of silicate magma ascent as a result of S solubility increase in the magma (Kerr and Leitch, 2005) due to decreasing pressure (Mavrogenes and O'Neill, 1999). Therefore, while sulfide dissolution may be taking place, there may also be a co-existing telluride melt which should scavenge almost all the Pd (and Au and Ag) originally present in the sulfide melt droplets (Helmy et al., 2007; Holwell and McDonald, 2010). These Au-Ag-Pd-telluride melts could remain as droplets of immiscible liquid down to low temperatures (~400 °C) in both silicate magma and hydrothermal fluids in an ample window of fO_2–fS_2 (Markham, 1960; Cabri, 1965; Kracek et al., 1966; Helmy et al., 2007; Tesfaye et al., 2013; Keith et al., 2020). Thus, while Pd and most of the Au and Ag was likely transported by telluride melt, Cu along with other metals (e.g., Fe) should be redissolved into the silicate magma, which upon cooling generates Cu-rich hydrothermal fluids (e.g., Halter et al., 2005; Cocker et al., 2016; Holwell et al., 2019).

Perhaps the most intriguing evidence on the origin of sulfide melts and their related Au–Ag–Pd-telluride melts at Elatsite come from isotopic studies (Sr, Nd, Pb and Hf), which show that alkali melts parental to all types of porphyry rocks within the Elatsite deposit, originated from an enriched mantle source with variable crustal contamination (von Quadt et al., 2002; Stoykov et al., 2004). Georgiev (2008) suggested a mantle-derived origin for the methane present in two-phase (CO_2-CH_4) high-temperature (> 500 °C) fluid inclusions previously identified by Strashimiriov et al. (2002) in the Elatsite deposit. These types of fluid inclusions suggest that carbon, as a buoyant supercritical CO_2 fluid, could be present in the primitive Elatsite magmas acting as covert agent aiding and promoting the physical transport of sulfides and/or telluride melt droplets (Blanks et al., 2020). In addition, the presence of Co−Ni minerals found in the Elatsite deposit, which are very unusual in porphyry systems, may suggest a contribution from mafic/ultramafic sources (Strashimiriov et al., 2002). Popov and Georgiev (2004) ruled out a contribution of Co and Ni from nearby

and/or country-host rocks of the deposit. Augé et al. (2005) interpreted this "mafic" assemblage as an evidence of derivation of the Elatsite parental melts directly from the upper mantle. Hanley and MacKenzie (2009) and Hanley et al. (2010) documented that PGE incorporation into pyrite was coincident to Co−Ni enrichment during high temperature hydrothermal events, pre-dating Cu (and Au) precipitation in porphyries from British Columbia. They also interpreted that such Co−Ni enrichment fingerprints a mafic contributor to the PGE tenor of the deposits. In a previous work, Thompson et al. (2001) also identified "mafic" contributor in the porphyries from British Columbia to explain the origin of PGE enrichment in these porphyry deposits. These latter authors interpreted that such contributor was an enriched-source region in the mantle from which the parental alkaline magmas of these deposits were extracted. It is important to note that Hanley et al. (2010) also reported glassy inclusion within leucititic, high Mg basalt flows, coeval with the porphyry rocks in the deposits of British Columbia, preserving Pd/Pt ratios of the same order of magnitude as in the bulk mineralization. According to these authors, PGE-rich magmas were extracted from the mantle to the place of deposition by a mechanism by which they experienced limited fractionation of Pd from Pt during melt fractionation or mixing, melt ascent, fluid exsolution, and pyrite precipitation. These results are consistent with recent observations by Holwell et al. (2019), who have noted that upper crustal porphyry-epithermal ore systems worldwide share a common metallogenic signature, with anomalously high amounts of Au-Te-rich magmatic sulfides when there is a contribution of alkaline magmas derived metasomatized mantle during subduction zone magmatism. They suggested that a trans-litospheric continuum exists whereby (post)-subduction magmas, transporting metal-rich sulfide cargo play a fundamental role in fluxing metals into the crust from metasomatized lithospheric mantle. Interestingly, the existence of trans-lithospheric faults that favored the ascent of mantle-derived magma has been suggested for the Late Cretaceous magmatism that produced the Elatsite ores either in a trans-tensional context originated during an active subduction zone (Gallhofer et al., 2015; Menant et al., 2018; Baker, 2019) or post-subduction after orogenic collapse (Nebauer and Heinrich, 2003; Halter et al., 2005; Chambefort and Moritz, 2006; Georgiev, 2008).

6.3. Noble metals in high-temperature bornite and chalcopyrite

Chalcopyrite and bornite from the *quartz–magnetite–bornite–chalcopyrite* assemblage analyzed here are significantly impoverished in Au (< 0.08 ppm) and Ag (< 220 ppm), consistent with previous data obtained by Cook et al. (2011) and George et al. (2018). Chalcopyrite and bornite in other hypogene ores from PCDs (e.g., Batu Hijau in Indonesia; Arif and Baker, 2004) are also poor Au-carriers (Fig. 9). However, chalcopyrite and bornite from hypogene ores from PCDs worldwide usually contain higher amounts of Ag, 500–5000 ppm (Arif and Baker, 2004; Cioaca et al., 2014; George et al., 2016, 2018). As noted above, the relatively Au- and Ag-poor nature of the (Cu−Fe)-rich sulfides analyzed here could be explained by the sequestration of both noble metals by immiscible semimetal-rich melt(s) segregated earlier than the hydrothermal deposition of the Cu-sulfides.

The analyzed chalcopyrite and bornite contains almost no detectable amounts of Pt, but significant amount of Pd (up to ~5 ppm in bornite and up to 3 ppm in chalcopyrite). To the best of our knowledge, there are no available data of Pd in chalcopyrite and bornite of hypogene ores from PCDs obtained by means of accurate micro-analytical techniques (i.e., SIMS, PIXE, LA-ICPMS). However, available data for (Cu−Fe)-rich from magmatic ore-systems indicate that Pd, like Te and Bi, is incompatible in high-temperature intermediate solid solution (iss) as well as their low-temperature products (e.g., chalcopyrite and bornite) (e.g., Helmy et al., 2007; Dare et al., 2014). Rather, Pd usually combines with these semimetals, if available, to form discrete PGM (e.g., Holwell and Mcdonald, 2010). At Elatsite, this predicted magmatic behavior is confirmed by the fact that bornite typically hosts micron-sized inclusions of Pd-telluride grains, visible under the optical microscope (Fig. 3a–l). A careful examination of the time-resolved spectra signals, collected during LA-ICP-MS, reveal abundant $^{106}Pd–^{125}Te$ spikes (e.g., Fig. 7b and d), confirming the presence of individual particles or aggregates of micro- to nano-particulate Pd−Te, hosted in bornite and chalcopyrite too. The results presented here indicate that Pd does not enter in solid solution with (Cu−Fe)-rich sulfides, but it is preferentially concentrated into micro- to nano-sized particles of Pd−Te, formed from immiscible telluride melts.

6.4. Secondary Au−Pd enrichment in low-temperature pyrite

Gold contents in the analyzed pyrite from Elatsite (~3 ppm on average) overlap the range of values reported for Au in solid solution in pyrite from porphyry/epithermal ores of some PCDs worldwide, such as Mount Polley in Canada (Pass, 2010), Dexing in China (< 10 ppm Reich et al., 2013), Pebble in Alaska (~4 ppm; Gregory et al., 2013) and Lihir in Papua New Guinea (~0.5 ppm; Sykora et al., 2018) (Fig. 9). However, it is considerably lower than reported for pyrite from Buchim PCD in Macedonia (~7 wt%; Serafimosvski et al., 2013) or PCD from the Metaliferi Mountains in Romania (~160 ppm; Cioaca et al., 2014), but higher than Agua Rica in Argentina and porphyry deposits in the Urumieh-Dokhtar arc, Iran (the Meiduk, Iju, Sarkuh, Dalli, Chahfiruzeh, and Keder deposits) (i.e., sub-ppm levels; Franchini et al., 2015; Zarasvandi et al., 2018) (Fig. 9).

At Elatsite, gold contents of pyrite correlate positively with As contents (Fig. 8b). These high concentrations of As detected in pyrite grains of up to ~19 wt% (Appendices A and C) are consistent with previous reports for pyrite at Elatsite (e.g., Krumov et al., 2016), and classify them as "arsenian" in terms of As contents. A similar positive Au−As correlation in pyrite has already been reported for (Au, As)-bearing pyrite from other hydrothermal-related deposits worldwide (Cook and Chryssoulis, 1990; Fleet et al., 1993; Reich et al., 2005; Large et al., 2009; Franchini et al., 2015; Deditius and Reich, 2016; Sykora et al., 2018; Zarasvandi et al., 2018). It reflects the impact of arsenic in the speciation of Au in pyrite, i.e., incorporation either into the lattice as $Au^{1+}–As^{-1}$ solid solution or as micro- to nano-sized inclusions of Au-bearing minerals (Reich et al., 2005; Cook et al., 2013). A preliminary analysis of gold speciation in pyrite can be performed using the Au−As saturation curves at 150–250 °C (Reich et al., 2005) and 300–500 °C (Deditius et al., 2014) in plots Au vs. As (Fig. 10). According to Reich et al. (2005) and Deditius et al. (2014), Au−As points that plot below the solubility curves should contain Au in solid solution, whereas those plotting above the solubility line should have Au present as inclusions. In this graph, all data for Elatsite pyrite, plot below the Au solubility curve of 150–250 °C, a temperature relevant for the formation of the *quartz–galena–sphalerite* assemblage at Elatsite (i.e., 240–230 °C; Strashimiriov et al., 2002). Therefore, one could expect that Au was contained within the crystal lattice of the pyrite grains. This is consistent with the fact that most of the analyzed pyrite does not contain micro- to- nano-sized inclusions visible under FE-SEM and with the relatively homogenous Au-signal for time-resolved spectra, collected during LA-ICP-MS analysis of pyrite (Fig. 7e). Nevertheless, some of the time-resolved spectra are characterized by spiky Au-Sb-As signal, suggesting the presence of micro- to- nano-sized inclusions of Au too (Fig. 7f). Moreover, Dragov and Petrunov (1996) reported Au minerals associated with pyrite of this assemblage, although they did not provide an accurate textural description for such gold-pyrite association. Therefore, it is possible that Au in the Elatsite pyrite occurs in two mineralogical forms, i.e., structurally bound ions (Au^{1+}) and as free particles of Au-bearing minerals. However, additional HRTEM studies are necessary to better characterize the nature of these gold-bearing nano-particles and the relation with their host sulfide matrices.

As documented above, field evidence and mineralogical studies indicate that pyrite-bearing veins of the *quartz–galena–sphalerite* assemblage were formed at the latest ore mineralizing porphyry-to-
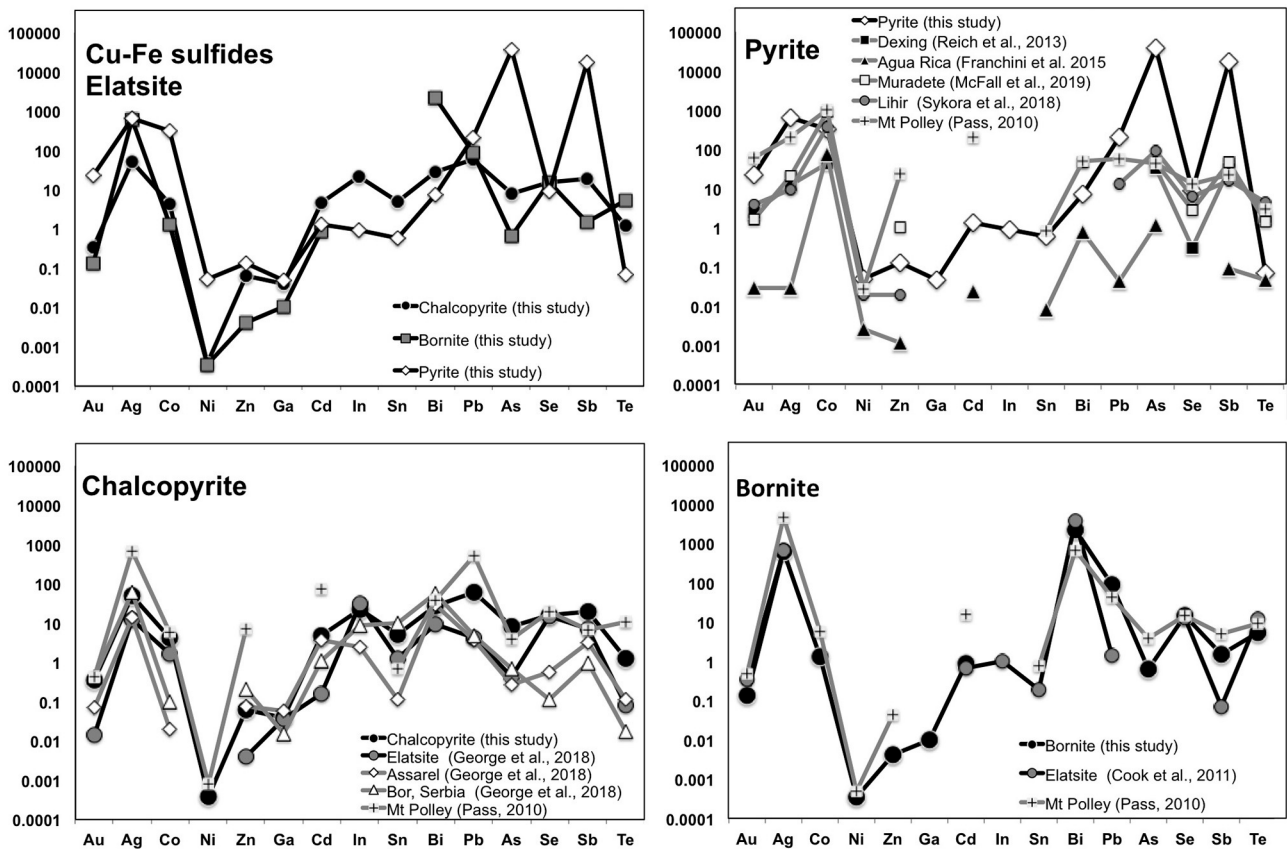
Fig. 9. Trace element spidergrams (average concentrations) of the sulfides analyzed in this study from Elatsite and comparison with equivalents from porphyry-epithermal ores of PCDs worldwide. References are inset in the figure.
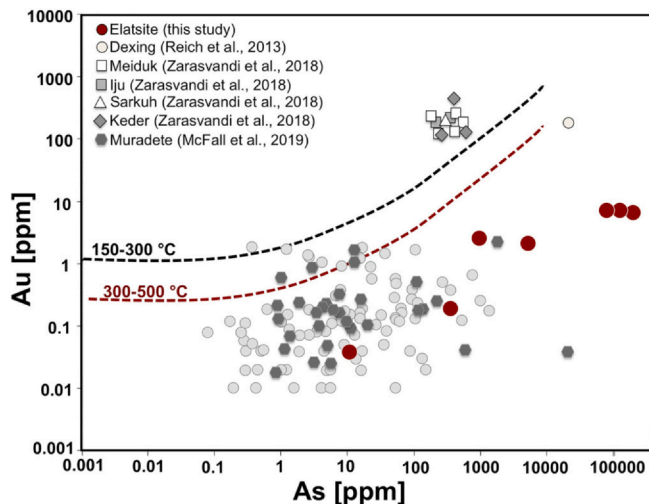

Fig. 10. Laser ablation-inductively coupled plasma-mass spectrometry (LA-ICP-MS) analyses of pyrite grains from the epithermal *quartz–galena–sphalerite* assemblage at Elatsite compared to LA-ICP-MS analyses of pyrite samples from global porphyry deposits. References are inset in the figure.

epithermal event at Elatsite, and they were produced as a result of re-mobilization of metals from earlier ore mineral assemblages (Strashimirov et al., 2002; Popov and Georgiev, 2004; Georgiev, 2008). In this scenario, high Au concentrations in the analyzed pyrite may be the result of an effective scavenging and redistribution process whereby Au was lost from pre-existing sulfides and re-deposited during the latest low-temperature alteration ore-forming stage active in the porphyry ore-system. Moreover, the positive correlation of Au with Ag as well as

other semi-metals (Sb) and base-metals (Zn, Cd, In and Pb) suggest that these low-temperature fluids were also effective in transporting all these elements along with Au. Consistently, the contents of Ag (up to 242 ppm) and Sb (~2800 pm on average) in Elatsite pyrite exceed those reported for high-temperature pyrite from other porphyry Cu-Mo-Au deposit < 50 ppm (Reich et al., 2013; McFall et al., 2018; Cioaca et al., 2014; Franchini et al., 2015). Conversely, pyrite grains from these deposits have higher Zn (> 200–7000 ppm at Muradate; McFall et al., 2019) than Elatsite pyrite analyzed here (< 150 ppm). These observations confirm previous observations that As exerts an important role in favoring the entering of other elements such as Ag, Sb, Cd, In, Pb in solid solution in the pyrite structure (Pass, 2010; Deditius and Reich, 2016).

In Elatsite pyrite grains, however, there is no positive correlation of Au and As with Bi or Te as observed in pyrite from other PCDs, suggesting a little role of these elements in controlling gold partitioning into pyrite precipitating at the latest stages of hydrothermal alteration in the porphyry ore-system. The concentrations of Bi (< 5 ppm) and Te (< 0.3 ppm) are lower than the range reported for pyrite from other PCDs (~50–100 ppm), whereas for Co (< 900 ppm) and Ni (< 1600 ppm) are similar (Fig. 9; Reich et al., 2013; Cioaca et al., 2014; Franchini et al., 2015; McFall et al., 2019). These trace elements are most likely hosted within the pyrite structure as stoichiometric substitutions, such as Co^{2+} and Ni^{2+} for Fe^{2+} and possibly Te^{2-} for S^{2-} (McFall et al., 2019 and references therein). Of particular interest is the Co/Ni ratio, as pyrite crystallized from high-temperature hydrothermal fluids or magmas usually exhibit ratios > 10 (Bralia et al., 1979; Hanley and MacKenzie, 2009; Gregory et al., 2013; Reich et al., 2013; Zhang et al., 2016). The pyrite studied here exhibits contents of Ni higher than Co (Co/Ni = 0.1–0.6), which is consistent with its origin related to relatively low-temperature hydrothermal fluids.

On the other hand, LA-ICP-MS analysis on pyrite yield up to ~5 ppm Pd and 0.14 ppm Pt (Appendix C); the inspection of the time-resolved spectra collected during LA-IPC-MS analyses of these pyrite grains (not shown in figures) suggest that these elements are hosted in solid solution. Pašava et al. (2010) also found significant amount of PGE in pyrite from a similar pyrite-sphalerite assemblage from the Kalmakyr porphyry Cu–Au–Mo deposit. They noted that such pyrite formed in the mineralizing porphyry-stage contained Pd and Pt below detection limits. These results contrast, however, with previous ones acquired by Hanley and MacKenzie (2009) and Hanley et al. (2010) for (Ni−Co)-rich pyrite from alkali porphyry Cu−Au deposits from the Canadian Cordillera, which contains up to 90 ppm Pd and 20 ppm Pt. Interestingly, these pyrites were found forming part of a mineral assemblage predating veining of the porphyry-stage. More recently, Serafimosvski et al. (2013) have reported As-rich pyrite with up to ~6.5 wt% Pd, although these analyses were obtained using EPMA. It is also worth to note that contents of Pd and Pt detected in some pyrites from PCDs are much higher than reported for magmatic pyrite in Ni-Cu ± PGE deposits, which show sub-ppm levels of Pd and Pt (Dare et al., 2011; Piña, 2019). High amounts of Pd and Pt in (Ni−Co)-rich pyrites formed at high-temperatures in PCDs could be related with a crystallographic (substitution) mechanism whereby the partitioning of Pd and Pt into pyrite is promoted during high temperature crystallization of pyrite when Fe^{2+} site vacancies in the pyrite lattice are maximized (e.g., Hanley et al., 2010). However, this interpretation must be ruled out for the Elatsite pyrite formed by low-temperature fluids. We suggest that Pd and, at a lesser extent Pt, like Au, were incorporated into pyrite by hydrothermal fluids that leached pre-existing veins already enriched in (Pd−Pt)-bearing minerals, e.g., the *quartz–magnetite–bornite–chalcopyrite* assemblage. Experimental results indicate that hydrothermal remobilization of Pd and Pt at Elatsite is a very plausible mechanism (e.g., Xiong and Wood, 2000), particularly if one considers the nature of fluid inclusion preserved in both opaque and gangue ores of the *quartz–galena–sphalerite* assemblage. These fluid inclusions preserve evidence of low-saline and temperature (240–230 °C) fluids which could effectively transport Pd (and Pt) (see Xiong and Wood, 2000), along with Au, Sb, As, Pb and S, and late precipitate Pd-rich pyrite in equilibrium with sulfosalts (e.g., enargite), Ag-rich galena and sphalerite (Dragov and Petrunov, 1996; Georgiev, 2008).

7. Conclusions

Summarizing, we can conclude that our observations are consistent with previous mineralogical studies on Elatsite, confirming that noble metals such as Pd, Au, Ag were mostly incorporated during the earliest potassic alteration stage. We propose a novel mechanism in which the transport of noble metals like Pd, Au and Ag, and subsequent deposition of minute grains of these noble metals did not take place solely as dissolved species in the high-temperature hydrothermal fluid, as all previous authors suggested. Rather, there are compelling evidence that noble metals (PGE, Au, Ag) were collected by droplets of Te-rich melt, physically entrained in the high-temperature hydrothermal fluid responsible for the potassic alteration and precipitation of the quartz–magnetite–bornite–chalcopyrite assemblage at Elatsite. This telluride melt stripped most of the noble metals giving rise to complex mineral assemblages of PGE, Au and Ag while leaving behind a hydrothermal fluid depleted in these elements, which deposited noble metal-poor (Cu−Fe)-rich sulfides.

Supplementary data to this article can be found online at https://doi.org/10.1016/j.gexplo.2020.106664.

CRediT authorship contribution statement

This work include contributions from all the authors who have worked as a team collecting samples, acquiring data and sourcing ideas that inspired the interpretations and models provided in this manuscript. Finally, all the authors revised the writing style of the manuscript. Specifically, J.M.G.-J., F.G. and J.P. conceived and designed the study while T.N.K. provided the samples. The EMPA and SEM analytical work was carried out largely by J.M.G.-J, I.B. and F.T. whereas the in situ analysis of sulfides at University of Chicoutimi was carried out by R.P. The thin-foil preparation by FIB was carried out by J.F·P with collaboration of J.R whereas the HRTEM study at University of Granada was carried out by J.M.G.-J under the supervision and guidance of FN. All the authors analyzed and discussed the data, and revised the manuscript, which was written by J.M.G.-J. and F.T.

Declaration of competing interest

We would like to let know that we don't have conflict of interest.

References

Afifi, A.M., Kelly, W.C., Essene, E.J., 1988. Phase relations among tellurides, sulfides, and oxides: I. Thermochemical data and calculated equilibria; II. Applications to telluride-bearing ore deposits. Economic Geology 83 377-394 and 395-404.

Aird, H.M., Bermudez, J., Purcell, C., Matthews, J., de Witt, N., Meisel, Z., 2019. Trace metal microparticles hosted by sulfides in the Ann Mason porphyry copper deposit, Yerington, Nevada. In: American Geophysical Union, Fall Meeting 2019, abstract #V31B-03.

Aminzadeh, B., Shahabpour, J., Maghami, M., 2011. Variation of rhenium contents in molybdenites from the Sar Cheshmeh porphyry Cu–Mo deposit in Iran. Resour. Geol. 61, 290–295.

Arif, J., Baker, T., 2004. Gold paragenesis and chemistry at Batu Hijau, Indonesia: implications for gold-rich porphyry copper deposits. Mineral. Deposita 39, 523–535.

Augé, T., Petrunov, R., Bailly, L., 2005. On the origin of the PGE mineralization in the Elatsite porphyry Cu-Au deposit, Bulgaria: comparison with theBaula-Nuasahi complex India, and other alakine PGE-rich porphyries. Can. Mineral. 43, 1355–1372.

Baker, T., 2019. Gold ± copper endowment and deposit diversity in the western Tethyan magmatic belt, Southeast Europe: implications for exploration. Economic Geology 114, 1237–1250.

Berzina, A.N., Sotnikov, V.I., Economou-Eliopoulos, M., Eliopoulos, D.G., 2005. Distribution of rhenium in molybdenite from porphyry Cu-Mo and Mo-Cu deposits of Russia (Siberia) and Mongolia. Ore Geol. Rev. 26 (1–2), 91–113.

Berzina, A.N., Sotnikov, V.I., Economou-Eliopoulos, M., Eliopoulos, D.G., 2007. First finding of merenskyite (Pd,Pt)Te₂ in porphyry Cu-Mo ores in Russia. Russian Geology and Geophysics 48, 656–658. https://doi.org/10.1016/j.rgg.2007.07.001.

Blanks, D.E., Holwell, D.A., Fiorentini, M.L., Moroni, M., Giuliani, A., Tassara, S., Gonzalez-Jimenez, J.M., Boyce, A.J., Ferrari, E., 2020. Fluxing of mantle carbon as a physical agent for metallogenic fertilisation of the crust. Nat. Commun. 11, 342.

Bogdanov, B., 1986. Copper ore deposits in Bulgaria. Schriftenreihe der Erdwissenschaftlichen Kommissionen by Osterreichische Akademie der Wissenschaften 8, 103–112.

Bogdanov, B., 1987. Copper deposits in Bulgaria. Technica, Sofia 388 p. (in Bulgarian).

Bogdanov, K., Filipov, A., Kehayov, R., 2000. Pd and Au Mineralization in the Porphyry-Copper Deposit Elatsite, Bulgaria. - ABCD-GEODE 2000, Bulgaria, Abstracts, ABCD-Geode 2000 Workshop, Borovets, May 2000. pp. 11.

Bogdanov, K., Filipov, A., Kehayov, R., 2005. Au-Ag-Te-Se minerals in the Elatsite porphyry-copper deposit, Bulgaria. Geochem. Mineral. Petrol. 14–19.

Bralia, A., Sabatini, G., Troja, F., 1979. A revaluation of the Co/Ni ratio in pyrite as geochemical tool in ore genesis problems. Mineral. Deposita 14, 353–374.

Brugger, J., Etschmann, B.E., Grundler, P.V., Weihua, L., Testemale, D., Pring, A., 2012. XAS evidence for the stability of polytellurides in hydrothermal fluids up to 599 °C,

800 bar. Am. Mineral. 97, 1519–1522. https://doi.org/10.2138/am.2012.4167.

Cabri, L.J., 1965. Phase relations in the Au-Ag-Te system and their mineralogical significance. Econ. Geol. 60, 1569–1606.

Cabri, L.J., 1981. Platinum-Group Elements: Mineralogy, Geology, Recovery. Published for the Geology division of CIM by the Canadian Institute of Mining and Metallurgy.

Cepedal, A., Fuertes-Fuente, M., Martín-Izard, A., González-Nistal, S., Rodríguez-Pevida, L., 2006. Tellurides, selenides and Bi-mineral assemblages from the Río Narcea Gold Belt, Asturias, Spain: genetic implications in Cu–Au and Au skarns. Mineralogy and Petrology 87, 277–304. https://doi.org/10.1007/s00710-006-0127-7.

Chambefort, I., Moritz, R., 2006. Late Cretaceous structural control and Alpine overprint of the high-sulfidation Cu–Au epithermal Chelopech deposit, Srednogorie belt, Bulgaria. Mineralium Deposita 41, 259–280.

Chattopadhyay, G., Bhatt, Y.J., Khere, S.K., 1986. Phase diagram of the Pd-Te system. Journal of the Less-Common Metals 123, 251–266.

Chiaradia, M., 2014. Copper enrichment in arc magmas controlled by overriding plate thickness. Nat. Geosci. 7, 43–46.

Cioaca, M.E., Munteanu, M., Qi, L., Costin, G., 2014. Trace element concentrations in porphyry copper deposits from Metaliferi Mountains, Romania: a reconnaissance study. Ore Geol. Rev. 63, 22–39.

Ciobanu, C., Cook, N., 2002. Tellurides, selenides (and Bi-sulphosalts) in gold deposits. In: Extended Abstracts, 11thQuadrennial IAGODS ymposium Windhoek, Namibia, July 2002.

Ciobanu, C.L., Cook, N.J., Pring, A., 2005. Bismuth tellurides as gold scavengers. In: Mao, J.W., Bierlein, F.P. (Eds.), Mineral Deposit Research: Meeting the Global Challenge. New York, Springer, Berlin, Heidelberg, pp. 1387–1390.

Ciobanu, C.L., Cook, N.J., Damian, F., Damian, G., 2006. Gold scavenged by bismuth melts: an example from Alpine shear-remobilizations in the Highis Massif, Romania. Mineralogy and Petrology 87, 351–384.

Ciobanu, C., Birch, W.D., Cook, N.J., Pring, A., Grundler, P.V., 2010. Petrogenetic significance of Au–Bi–Te–S associations: the example of Maldon, Central Victorian gold province, Australia. Lithos 116, 1–17.

Ciobanu, C.L., Cook, N.J., Kelson, C.R., Guerin, R., Kalleske, N., Danyushevsky, L., 2013. Trace-element heterogeneity in molybdenite fingerprints stages of mineralization. Chem. Geol. 347, 175–189.

Cocker, H.A., Valente, D.L., Park, J.-W., Campbell, I.H., 2016. Using platinum group elements to identify sulfide saturation in a porphyry Cu system: the El Abra porphyry Cu deposit, Northern Chile. Journal of Petrology 56, 2491–2514.

Cook, N.J., Chryssoulis, S.L., 1990. Concentrations of "invisible gold" in common sulfides. Can. Mineral. 28, 1–16.

Cook, N.J., Ciobanu, C.L., 2004. Bismuth tellurides and sulphosalts from the Larga hydrothermal system, Metaliferi Mts., Romania: paragenesis and genetic significance. Mineral Magazine 68, 301–321.

Cook, N.J., Ciobanu, C.L., Danyushevsky, L.V., Gilbert, S., 2011. Minor and trace elements in bornite and associated Cu–(Fe)–sulfides: LA-ICP-MS study. Geochim. Cosmochim. Acta 75, 6473–6496.

Cook, N.J., Ciobanu, C.L., Meria, D., Silcock, D., Wade, B., 2013. Arsenopyrite–pyrite associ- ation in an orogenic gold ore: tracing mineralization history from textures and trace elements. Econ. Geol. 108, 1273–1283.

Core, D.P., Kesler, S.E., Essene, E.J., 2006. Unusually Cu-rich magmas associated with giant porphyry copper deposits: evidence from Bingham. Utah Geol. 34, 41–44.

Crespo, J., Reich, M., Barra, F., Verdugo, J.J., Martínez, C., 2018. Critical metal particles in copper sulfides from the supergiant Río Blanco Porphyry Cu–Mo deposit, Chile. Minerals 8, 519.

Dare, S.A.S., Barnes, S.-J., Prichard, H.M., Fisher, P.C., 2011. Chalcophile and platinum-group element (PGE) concentrations in the sulfide minerals from the McCreedy East deposit, Sudbury, Canada, and the origin of PGE in pyrite. Mineral. Deposita 46, 381–407.

Dare, S.A.S., Barnes, S.-J., Prichard, H.M., Fisher, P.C., 2014. Mineralogy and geochemistry of Cu-rich ores from the McCreedy East Ni-Cu-PGE deposit (Sudbury, Canada): implications for the behavior of platinum Group and chalcophile elements at the end of crystallization of a sulfide liquid. Econ. Geol. 109, 343–366. https://doi.org/10.2113/econgeo.109.2.343.

David, V., Timms, D., 2018. Cargo Porphyry Cu-Au Deposit – Where Is the High Grade Core?, ASEG Extended Abstracts, 2018. 1. pp. 1–7. https://doi.org/10.1071/ASEG2018abM3_1D.

Deditius, A.P., Reich, M., 2016. Constraints on the solid solubility of Hg, Tl, and Cd in arsenian pyrite. American Mineralogist 101, 1451–1459.

Deditius, A.P., Utsunomiya, S., Reich, M., Kesler, S.E., Ewing, R.C., Hough, R., Walshe, J., 2011. Trace metal nanoparticles in pyrite. Ore Geol. Rev. 42, 32–46.

Deditius, A.P., Reich, M., Kesler, S.E., Utsunomiya, S., Chryssoulis, S.L., Walshe, J., Ewing, R.C., 2014. The coupled geochemistry of Au and As in pyrite from hydrothermal ore deposits. Geochim. Cosmochim. Acta 140, 644–670.

Dimitrov, S., 1988. Mineral compositions on pluton- desseminated Mo-Cu deposit Elatsite. Annual of the Committee of Geology in Bulgaria 28, 67–84 (in Bulgarian with French abstract).

Dimitrov, S., Koleva, E., 1975. On the presence of platinum group elements in some copper deposits in Bulgaria. Ore Forming Processes and Mineral Deposits 3, 15–19 (in Bulgarian with English abstract).

Douglas, N., 2000. The liquid bismuth collector model: an alternative gold deposition mechanism. In: Geological Society of Australia Abstracts. Geological Society of Australia. vol. 1999. pp. 135.

Dragov, P., Petrunov, R., 1996. Elatsite porphyry copper-precious metals (Au and PGE) deposit. In: Popov, P. (Ed.), Plate tectonic aspects of the Alpine metallogeny in the Carpatho- Balkan region. Proc Annu Meet UNESCO-IGCP Proj 356, Sofia. vol 1. Bulgarian Academy of Science, Sofia, pp. 171–174.

Economou-Eliopoulos, M., 2005. Exploration for deposits of platinum-group elements.

Mineral. Assoc. Canada Short Course 35 (35), 203–246.

Economu-Eliopoulos, M., Eliopoulos, D.G., 2000. Palladium, platinum and gold concentra tion in porphyry copper systems of Greece and their genetic significance. Ore Geol. Rev. 16, 59–70.

Eliopoulos, D., Economou-Eliopoulos, M., Zelyaskova-Panayiotova, M., 2014. Critical factors controlling pd and pt potential in porphyry Cu–Au deposits: evidence from the Balkan Peninsula. Geosciences 4, 31–49. https://doi.org/10.3390/geosciences4010031.

Farrow, C.F.G., Watkinson, D.H., 1992. Alteration and the role of fluids in Ni, Cu, and platinum-group element deposition, sudbury igneous complex contact, Onaping-Levack area, Ontario. Mineral. Petrol. 46, 67–83.

Fleet, M.E., Chryssoulis, S.L., MacLean, P.J., Davidson, R., Weisener, C.G., 1993. Arsenian pyrite from gold deposits; Au and As distribution investigated by SIMS and EMP, and color staining and surface oxidation by XPS and LIMS. Can. Mineral. 31, 1–17.

Franchini, M., McFarlane, C., Maydagán, L., Reich, M., Lentz, D.R., Meinert, L., Bouhier, V., 2015. Trace metals in pyrite and marcasite from the Agua Rica porphyry-high sulfidation epithermal deposit, Catamarca, Argentina: Textural features and metal zoning at the porphyry to epithermal transition. Ore Geol. Rev. 66, 366–387.

Gallhofer, D., von Quadt, A., Peytcheva, I., Shmid, S.M., Heinrich, C.A., 2015. Tectonic, magmatic, and metallogenic evolution of the Late Cretaceous arc in the Carpathian-Balkan orogeny. Tectonics 34, 1813–1836.

George, L.L., Cook, N.J., Ciobanu, C.L., 2016. Partitioning of trace elements in co-crystallized sphalerite-galena-chalcopyrite hydrothermal ores. Ore Geol. Rev. 77, 97–116.

George, L.L., Cook, N.J., Crowe, B.B.P., Ciobanu, C.L., 2018. Trace Elements in Hydrothermal Chalcopyrite.

Georgiev, G., 2008. A genetic model of the Elatsite porphyry copper deposit. Geochemistry, Mineralogy and Petrology Sofia 46, 143–160.

Grabezhev, A.I., 2013. Rhenium in porphyry copper deposits of the urals. Geology Ore Deposits 55, 13–26.

Gregory, M.J., Lang, J.R., Gilbert, S., Hoal, K.O., 2013. Geometallurgy of the Pebble porphyry Cu-Au-Mo deposit, Alaska: implications for gold distribution and paragenesis. Economic Geology108 463–482.

Griffin, W.L., Begg, G.C., O'Reilly, S.Y., 2013. Continental-root control on the genesis of magmatic ore deposits. Nat. Geosci. 6, 905–910.

Guimarães, F.S., Cabral, A.R., Lhemann, B., Rios, F.J., Ávila, M.A.B., Paulo de Castro, M., Queiroga, G.N., 2019. Bismuth-Melt Trails Trapped in Cassiterite–Quartz Veins. https://doi.org/10.1111/ter.12391.

Hadjyiski, G., Angelkov, K., Nedkova, Ts., Tsvetkova, H., 1970. Report for The Results From the Geological Exploration of Elatsite Copper-Ore Deposit – Etropole and Realized During 1959–1968 with Copper Reserves Calculation for Veinlet Impregnated Ore, in State at 01.07.1968. Ministry of Environment and Water, National Geofond, I-744. (in Bulgarian).

Halter, W.R., Heinrich, C.A., Pettke, R., 2005. Magma evolution and the formation of porphyry Cu-Au ore fluids: evidence from silicate and sulfide melt inclusions. Mineral. Deposita 39, 845–863.

Handy, M.R., Ustaszewski, K., Kissling, E., 2014. Reconstructing the Alps–Carpathians–Dinarides as a key to understanding switches in subduction polarity, slab gaps and surface motion. Int. J. Earth Sci. https://doi.org/10.1007/s00531-014-1060-3.

Hanley, J.J., MacKenzie, M., 2009. Incorporation of platinum-group elements and cobalt into subsidiary pyrite in alkalic Cu-Au porphyry deposits: significant implications for precious metal distribution in felsic magmatic-hydrothermal systems. In: AGU Spring Meeting Abstracts 2009. 2009 V14A-03.

Hanley, J.J., MacKenzie, M.K., Warren, M.R., Guillong, M., 2010. Distribution and origin of platinum-group elements in alkalic porphyry Cu–Au and low sulfidation epithermal Au deposits in the Canadian Cordillera. In: 11th International Platinum Symposium, June 21–24.

Heinrich, C.A., Neubauer, F., 2002. Cu–Au–Pb–Zn–Ag metallogeny of the Alpine–Balkan–Carpathian–Dinaride geodynamic province. Mineraium Deposita 37, 533–540.

Helmy, H.M., Ballhaus, C., Berndt, J., Bockrath, C., Wohlgemuth-Ueberwasser, C., 2007. Formation of Pt, Pd and Ni tellurides: experiments in sulfide-telluride systems. Contributions to Mineralogy and Petrology 153, 577–591. https://doi.org/10.1007/s00410-006-0163-7.

Helmy, H., Ballhaus, C., Fonseca, R., Leitzke, F., 2019. Arsenic, Te, Se and S Contents in Basaltic Melt at Arsenide, Telluride, Sulfide and Selenide Saturation: the Role of Metal Ligands and Implications for PGM Formation from Silicate Melts. Goldschmidt 2019 Conference.

Hoffman, E., Maclean, W.H., 1976. Phase relations of Michenerite and Merenskyite in the Pd-Bi-Te system. Econ. Geol. 71, 1461–1468.

Holwell, D.A., McDonald, I., 2010. A review of the behaviour of platinum group elements within natural magmatic sulfide ore systems. Platinum Metal Revoew 54, 26–36. https://doi.org/10.1595/147106709X480913.

Holwell, D.A., Fiorentini, M., McDonald, I., Lu, Y., Giuliani, A., Smith, D.J., Keith, M., Locmelis, M., 2019. A metasomatized lithospheric mantle control on the metallogenic signature of post-subduction magmatism. Nat. Commun. 10, 3511.

Hou, A., Wang, 2019. Fingerprinting metal transfer from mantle. Nature Communications 10, 3510.

Hou, Z., Zhou, Y., Wang, R., Zheng, Y., He, W., Zhao, M., Evans, N.J., Weinberg, R.F., 2017. Recycling of metal-fertilized lower continental crust: Origin of non-arc Au-rich porphyry deposits at cratonic edges. Geology 45, 563–566. https://doi.org/10.1130/G38619.1.

Ivanov, Z., Nedialkov, R., Bogdanov, K., 2014. Magmatic and ore-related breccias in the Elatsite porphyry-copper deposit (PCD) Bulgaria. Proceedings of XX CBGA Congress, Tirana, Albania, 24-26 September 2014. Bul. Shk. Gjeol. 1/2014, 158–161.

John, D.A., Taylor, R.D., 2016. By-products of porphyry copper and molybdenum deposits. Rev. Econ. Geol. 18, 137–164.

Kamenov, B., Yanev, Y., Bedialkov, R., Moritz, R., Peytcheva, I., von Quadt, A., Stoykov, S., Zartova, A., 2007. Petrology of Upper Cretaceous island-arc ore-magmatic centers from Central Srednogorie, Bulgaria: Magma evolution and paths. Geochemistry, Mineralogy and Petrology Sofia 45, 39–77.

Kanazirski, M., Chipchakova, S., Gorova, M., Arnaudova, R.R., 2002. Wallrock alterations in the porphyry copper deposits of the Panagyurishte ore district and formation–facial belonging of the metasomatites. Geologica Balkanica 32 (2–4), 77–80.

Kehayov, R., 2005. Mineral Assemblages of Gold and Conditions of There Formations in Elatsite Porphyry Copper Deposit. PhD Disertation. Sofia University, Sofia 208 p. (in Bulgarian).

Kehayov, R., Bogdanov, K., Fanger, L., von Quadt, A., Pettke, T., Heinrich, C., 2003. The fluid chemical evolution of the Elatsite porphyry Cu-Au-PGE deposit, Bulgaria. In: Eliopoulos et al. (Editors) 7th Bienial SGA meeting "Mineral Exploration and Sustainable Development" August 24–28, Athens, Greece, pp. 1173–1176.

Keith, M., Smith, D.J., Doyle, K., Holwell, D.A., Jenkin, G.R.T., Barry, T.L., Becker, J., Rampe, J., 2020. Pyrite chemistry: A new window into Au-Te ore-forming processes in alkaline epithermal districts, Cripple Creek, Colorado. Geochemica et Cosmochimica Acta 274, 172–191.

Kerr, A., Leitch, A.M., 2005. Self destructive sulfide segregation systems and the formation of high-grade magmatic ore deposits. Econ. Geol. 100, 311–332.

Kim, W.S., Chao, A.G., 1990. Phase relations in Pd–Te system. Journal of the Less-Common Metals 162, 61–74.

Koto, K., Morimoto, N., 1975. Superstructure investigation of bornite, Cu_5FeS_4, by the modified partial Patterson function locality: Cornwall, England. Acta Crystallographica, Section B 31, 2268–2273.

Kracek, F.C., Ksanda, C.J., Cabri, L.J., 1966. Phase relations in the system silver-tellurium. Am. Mineral. 51, 14–28.

Krumov, I.D., Bogdanov, K.B., Dimitrova, D.A., 2016. Trace Elements Vectors in Pyrite and Molybdenite from Elatsite PCD, Bulgaria. In: 2016 Society of Economic Geologists, Inc. SEG-MJD 2016 Conference.

Large, R.R., Danyushevsky, L., Hollit, C., Maslennikov, V.V., Meffre, S., Gilbert, S., Bull, S., Scott, R., Emsbo, P., Thomas, H., Singh, B., Foster, J., 2009. Gold and trace elements zonation in pyrite using Laser Imaging Technique: implications for the timing of gold in orogenic and Carlin-style sediment-hosted deposits. Econ. Geol. 104, 635–668.

Lee, C.T., Tang, M., 2020. How to make porphyry copeer deposits. Earth Planet. Sci. Lett. 529, 115868. https://doi.org/10.1016/j.epsl.2019.115868.

Lefort, D., Hanley, J., Guillong, M., 2011. Subepithermal Au-Pd mineralization associated with an alkalic porphyry Cu-Au deposit, Mount Milligan, Quesnel Terrane, British Columbia, Canada. Econ. Geol. 106, 781–808. https://doi.org/10.2113/econgeo. 106.5.781.

Lips, A.L.W., Herrington, R.J., Stein, G., Kozelj, D., Popov, K., Wijbrans, J.R., 2004. Refined timing of porphyry copper formation in the Serbien and Bulgarian portions of the Cretaceous Carpatho-Balkan Belt. Econ. Geol. 99, 601–609.

Liu, R., Chen, G., Yan, J., 2020. Compositions of Cu-(Fe)-sulfides in the 109 reduced granite-related Cu deposit, Xinjiang, Northwest China: Implications to the characteristics of ore-forming fluids. Geofluids, 7391369 11 pages. https://doi.org/10. 1155/2020/7391369.

Logan, J.M., Mihalynuk, M.G., 2014. Tectonic controls on Early Mesozoic paired alkaline porphyry deposit belts (Cu-Au ± Ag-Pt-Pd-Mo) within the Canadian Cordillera. Econ. Geol. 109, 827–858.

Magyarosi, Z., Watkinson, D.H., Jones, P.C., 2002. Mineralogy of Ni–Cu–platinum-group element sulfide ore in the 825 and 810 orebodies, Copper Clif South Mine, and P–T–X conditions during the formation of platinum-group minerals. Econ. Geol. 97, 1471–1486.

Makovicky, E., 2002. Ternary and quaternary phase systems with PGE. In: Cabri, L.J. (Ed.), The Geology, Geochemistry, Mineralogy and Mineral Beneficiation of Platinum-Group Elements. Canadian Institute of Mining, Metallurgy and Petroleum, Montreal, pp. 131–178.

Marchev, P., Kaiser-Rohrmeier, M., Heinrich, C., Ovtcharova, M., Von Quadt, A., Raicheva, E., 2005. Hydrothermal ore deposits related to post-orogenic extensional magmatism and core complex formation: the Rhodope Massif of Bulgaria and Greece. Ore Geol. Rev. 27, 53–89.

Markham, N.L., 1960. Synthetic and natural phases in the system Au-Ag-Te. Econ. Geol. 55, 1148–1178.

Matkovic, P., Schubert, K., 1978. Kristalstrtuktur von Pd_9Te_4. J Less-Common Metals 58, 39–46.

Mavrogenes, J.A., O'Neill, H.S.C., 1999. The relative effects of pressure, temperature and oxygen fugacity on the solubility of sulfide in mafic magmas. Geochim. Cosmochim. Acta 63, 1173–1180.

McCoy, D.T., 2000. Mid-Cretaceous Plutonic-Related Gold Deposits of Interior Alaska: Metallogenesis, Characteristics, Gold Associative Mineralogy and Geochronology. [Ph.D. Thesis]. University of Alaska, Fairbanks 245 p.

McFall, K.A., Naden, J., Roberts, S., Baker, T., Spratt, J., McDonald, I., 2018. Platinum-group minerals in the Skouries Cu-Au (Pd, Pt, Te) porphyry deposit. Ore Geol. Rev. 99, 344–364.

McFall, K., Roberts, S., McDonald, I., Boyce, A.J., Naden, J., Teagle, D., 2019. Rhenium enrichment in the muratdere Cu-Mo (Au-Re) porphyry deposit, Turkey: evidence from stable isotope analyses ($\delta^{34}S$, $\delta^{18}O$, δD) and laser ablation-inductively coupled plasma-mass spectrometry analysis of sulfides. Econ. Geol. 114, 1443–1466.

Menant, A., Jolivet, L., Tuduri, J., Loiselet, C., Bertrand, G., Guillou-Frottier, L., 2018. 3D subduction dynamics: a first-order parameter of the transition from copper- to gold-rich deposits in the eastern Mediterranean region. Ore Geol. Rev. 94, 118–135.

Mutschler, F.E., Griffen, M.E., Stevens, D.S., Shannon, S.S., 1985. Precious metal deposits

related to alkaline rocks in the North American Cordillera; an interpretive review. South African Journal of Geology 88, 355–377.

Nebauer, J., Greiner, B., Appel, E., 2001. Kinematics of the Alpine– West Carpathian orogen and palaeogeographic implications. Journal of Geological Society (London) 158, 97–110.

Neubauer, F., Heinrich, C., GEODE-ABCD Geodynamic Working Group, 2003. Late Cretaceous and Tertiary geodynamics and ore deposit evolution of the Alpine–Balkan–Carpathian– Dinaride orogen. In: Elioupolos, D.G. (Ed.), Mineral Exploration and Sustainable Development, Proceedings 7th Biennial SGA Meeting, Athens, Greece, 24–28 August 2003. Millpress Rotterdam, pp. 1133–1136.

Oberthür, T., Wiser, T.W., 2008. Gold-bismuth-telluride-sulphide assemblages at the Viceroy Mine, Harare-Bindura-Shamva greenstone belt, Zimbabwe. Mineralogical Magazine 72, 953–970.

Pašava, J., Vymazalová, A., Košler, J., Koneev, R.I., Jukov, A.V., Khalma- tov, R.A., 2010. Platinum-group elements in ores from the Kalmakyr por- phyry Cu-Au-Mo deposit, Uzbekistan: Bulk geochemical and laser ablation ICP-MS data. Mineralium Deposita 45, 411–418.

Pass, H.E., 2010. Breccia-Hosted Chemical and Mineralogical Zonation Patterns of the Northeast Zone, Mt. Polley cu-ag-au Alkalic Porphyry Deposit, British Columbia, Canada. PhD thesis. University of Tasmania.

Paton, C., Hellstrom, J., Paul, B., Woodhead, J., Hergt, J., 2011. Iolite: freeware for the visualisation and processing of mass spectrometric data. J. Anal. At. Spectrom. VL - IS. https://doi.org/10.1039/C1JA10172B. online.

Petrunov, R., 1995. Ore mineral paragenesis and zoning in the de- posit of Chelopech (in Bulgarian). Geochemistry Mineralogy and Petrology Sofia 30, 89–98.

Petrunov, R., Dragov, P., Ignatov, G., Neykov, H., Lliev, Ts, Vasileva, N., Tsadsov, V., Djunakov, S., Doncheva, K., 1992. Hydrothermal PGE-mineralisation in the Elacite porphyry copper deposit (the Sredna Gora metallogenic zone, Bulgaria). C RAcad Bulgare Sci 45 (4), 37–40.

Peytcheva, I., Von Quadt, A., Kouzmanov, K., Bogdanov, K., 2003. Timing of magmatism and mineralization in Elshitsa and Vlaykov Vruh Cu (Au) deposits of Central Srednogorie, Bulgaria: constraints from U–Pb zircon and rutile geochro- nology and Hf–zircon and Sr whole-rock tracing. In: Final GEODE-ABCD 2003 Workshop, Geodynamics and Ore Deposit Evolution of the Alpine–Balkan–Carpathian–Dinaride Province, Seggauberg, Austria, abstr vol. 46.

Piña, R., 2019. The Ni-Cu-(PGE) aguablanca ore deposit (SW Spain). In: Springer Briefs in World Mineral Deposits, pp. 78.

Plotinskaya, O.Y., Azovskova, O.B., Abramov, S.S., Groznova, E.O., Novoselov, K.A., Seltmann, R., Spratt, J., 2018. Precious metals assemblages at the Mikheevskoe porphyry copper deposit (South Urals, Russia) as proxies of epithermal overprinting. Ore Geol. Rev. https://doi.org/10.1016/j.oregeorev.2018.01.025.

Popov, K., Georgiev, G., 2004. Primary geochemical halo of "Elatsite" porphyry copper deposit. Минно-геоложки университет "Св. Иван Рилски" Годишник, том 47, свитък I, Геология и геофизика, София. pp. 119–124 стр.

Popov, P., Kovachev, V., 1996. Geology, composition and genesis of the mineralizations in the Central and Southern part of the Elatsite-Chelopech ore field. In: Popov, P. (Ed.), Plate Tectonic Aspects of the Alpine Metallogeny in the Carpato-Balkan region, UNESKO-IGCP Project No 356. Proccedings of the Annual Meeting, Sofia. 1. pp. 159–170.

Popov, P., Popov, K., 1997. Metallogeny of Pangyurishte ore region. In: Romic, K., Konzulovic, R. (Eds.), Proc Symp Ore Deposits Exploration, 2–4 April 1997, Belgrade, pp. 327–338.

Popov, P., Berza, T., Grubic, A., Ioane, D., 2000a. Late Cretaceous Apuseni-Banat-Timok-Srednogorie (ABTS) magmatic and metallogenic belt in the Carpathian-Balkan or- ogeny. Geologica Balcanica 32, 145–163.

Popov, P., Petrunov, V., Kovachev, S., Strashimirov, M., Kanazirski, M., 2000b. Elatsite-Chelopech ore field. In: Strashimirov, S., Popov, P. (Eds.), Geology and Metallogeny of the Panagyurishte Ore Region (Srednogorie Zone, Bulgaria). ABCD-GEODE Worksh, May 2000, Borovets. UMG St I Rilski. Guide Excursions A and C, Sofia, pp. 8–18.

Popov, P., Strashimirov, S., Popo, K., Petrunov, R., Kanazirski, M., Tzonev, D., 2003. Main features in geology and metallogeny of the Panagyurishte ore region. In: 50 Years Ann Univ Min Geol. 46. pp. 119–125.

Popov, P., Strashimirov, S., Popov, K., Kanazirski, M., Bogdanov, K., Radichev, R., Dimovski, S., Stoykov, S., 2012. Geology and Metallogeny of the Panagyurishte Ore Region. MGU, Sofia 228 p. (in Bulgarian with English extended abstract).

Rathkopf, C., Mazdab, F., Barton, I., Barton, M.D., 2017. Grain-scale and deposit-scale heterogeneity of Re distribution in molybdenite at the Bagdad porphyry Cu-Mo deposit, Arizona. Journal of Geochemical Exploration 178, 45–54.

Reich, M., Kesler, S.E., Utsunomiya, S., Palenik, C.S., Chryssoulis, S.L., Ewing, R.C., 2005. Solubility of gold in arsenian pyrite. Geochim. Cosmochim. Acta 69, 2781–2796.

Reich, M., Deditius, A., Chryssoulis, S., Li, J.-W., Ma, C.-Q., Parada, M.A., Barra, F., Mittermayr, F., 2013. Pyrite as a record of hydrothermal fluid evolution in porphyry copper system: a SIMS/EMPA trace element study. Geochim. Cosmochim. Acta 104, 42–62.

Richards, J.P., 2015. Tectonic, magmatic, and metallogenic evolution of the Tethyan orogen: from subduction to collision. Ore Geol. Rev. 70, 323–345.

Schmidt, S.M., Bernoulli, D., Fügenschuh, B., Matenco, L., Schefer, S., Schuster, R., Tischler, M., Ustaszewski, K., 2008. The Alpine–Car- pathian–Dinaridic orogenic system: correlation and evolution of tectonic units. Swiss J. Geosci. 101, 139–183.

Serafimovski, T., Blazev, K., Tasev, G., Pockov, K., 2013. Au-Pd bearing pyrites and chalcopyrites from the Buchim porphyry coper deposit, Eastern Macedonia. In: Mineral Deposit Research for a High-Tech World, 12th SGA Biennial Meeting 2013. Proceedings. Vol 2. pp. 876–879.

Sillitoe, R.H., 2010. Porphyry copper systems. In: Economic Geology. 105. pp. 3–41.

Sinclair, W.D., 2007. Porphyry deposits. In: Goodfellow, W.D. (Ed.), Geological

Association of Canada. Mineral Deposits Division, Special Publication, pp. 223–243.

Sinyakova, E.F., Kosyakov, V., Borisenko, A.S., Karmanov, N.S., 2019. Behavior of noble metals during fractional crystallization of Cu–Fe–Ni–(Pt, Pd, Rh, Ir, Ru, Ag, Au, Te) sulfide melts. Russ. Geol. Geophys. 60, 642–661. https://doi.org/10.15372/RGG2019050.

Smith, D.J., Naden, J., Jenkin, G.R.T., Keith, M., 2017. Hydrothermal alteration and fluid pH in alkaline-hosted epithermal systems. Ore Geol. Rev. 89, 772–779. https://doi.org/10.1016/j.oregeorev.2017.06.028.

Sotnikov, V.I., Berzina, A.N., Economou-Eliopoulos, M., Eliopoulos, D.G., 2001. Palladium, platinum and gold distribution in porphyry Cu - Mo deposits of Russia and Mongolia. Ore Geology Reviews 18, 95–111. https://doi.org/10.1016/S0169-1368(01)00018-X.

Stoykov, S., Peytcheva, I., von Quadt, A., Moritz, R., Frank, M., Fontignie, D., 2004. Timing and magma evolution of the Chelopech volcanic complex (Bulgaria). Schweiz. Mineral. Petrogr. Mitt. 84, 101–117.

Strashimirov, S., Ptrunov, R., Kanazirski, M., 2002. Porphyry-copper mineralization in the central Sred- nogorie zone. Mineral. Deposita 37, 587–598.

Summerlin, E., 2014. PGE Mineralization at the Allard Stock: Implications for the Porphyry to Epithermal Transition, La Plata Mountains, Colorado. Ph. D. Thesis. Auburn University, Alabama, USA (160 pp).

Sykora, S., Cooke, D.R., Meffre, S., Stephanov, A.S., Gardner, K., Scott, R., Selley, D., Harris, A.C., 2018. Evolution of pyrite trace element com- positions from porphyry-style and epithermal conditions at the Lihir gold deposit: implications for ore genesis and mineral processing. Econ. Geol. 113, 193–208.

Tarkian, M., Koopmann, G., 1995. Platinum-group minerals in the Santo Tomas II (Philex) porphyry copper-gold deposit, Luzon Island, Philippines. Mineralium Deposita 30, 39–47.

Tarkian, M., Stribrny, B., 1999. Platinum-group elements in por- phyry copper deposits: a reconnaissance study. Mineral. Petrol. 65, 161–183.

Tarkian, M., Hünken, U., Tokmakchieva, M., Bogdanov, K., 2003. Precious-metal dis- tribution and fluid-inclusion petrography of the Elatsite porphyry copper deposit, Bulgaria. Mineral. Deposita 38, 261–281.

Tesfaye, F., Taskinen, P., Aspiala, M., Feng, D., 2013. Experimental thermodynamic study of intermetallic phases in the binary Ag–Te system by an improved EMF method. Intermetallics 34, 56–62. https://doi.org/10.1016/j.intermet.2012.10.009.

Thompson, J.F.H., Lang, J.R., Stanley, C.R., 2001. Platinum group elements in alkaline porphyry deposits. British Columbia. Explor. Min. Br. Columbia Mines Branch Part B 57–64.

Toermanen, T.O., Koski, R.A., 2005. Gold enrichment and the Bi-Au association in pyr-rhotite-rich massive sulfide deposits, Escanaba Trough, Southern Gorda Ridge. Economic Geology and the Bulletin of the Society of Economic Geologists 100, 1135–1150.

Tokmakchieva, M., Pazderov, R., 1995. Mineral paragenesis of white metals in the composition of Elatsite deposit. Geology and mineral resources 5, 16–20.

Tooth, B., Brugger, J., Ciobanu, C., Liu, W., 2008. Modeling of gold scavenging by bis-muth melts coexisting with hydrothermal fluids. Geology 36, 815–818. https://doi.org/10.1130/G25093A.1.

Velásquez, G., Carrizo, D., Salvi, S., Vela, I., Pablo, M., Pérez, A., 2020. Tracking cobalt, REE and gold from a porphyry-type deposit by LA-ICP-MS: a geological approach towards metal-selective mining in tailings. Minerals 10, 109.

von Quadt, A., Peytcheva, I., Kamenov, B., Fanger, L., Heinrich, C.A., Frank, M., 2002. The Elatsite porphyry copper deposit in the Panagyurishte ore district, Srednogorie zone, Bulgaria: U–Pb zircon geochronology and isotope-geochemical investigations of magmatism and ore genesis. In: Blundell, D.J., Neubauer, F., von Quadt, A. (Eds.), The Tim- Ing and Location of Major Ore Deposits in an Evolving Orogen. vol. 204. *Geol. Soc. London Spec. Publ.*, pp. 119–135.

von Quadt, A., Moritz, R., Peytcheva, I., Heinrich, C., 2005. Geochronology and geody-namics of Upper Cretaceous mag- matism and Cu–Au mineralization in the Panagyurishte region of the Apuseni–Banat–Timok–Srednogorie belt (Bulgaria). Ore Geol. Rev. 27, 95–126.

Voronin, M.V., Osadchii, E.G., Brichkina, E.A., 2017. Thermochemical properties of silver tellurides including empressite (AgTe) and phase diagrams for Ag–Te and Ag–Te–O. Phys. Chem. Miner. 44, 639–653. https://doi.org/10.1007/s00269-017-0889-y.

Vymazalová, A., Laufek, F., Kristavchuk, A.V., Chareev, D.A., Drábek, M., 2015. The system Ag–Pd–Te: phase relations and mineral assemblages. Mineral Magazine 79, 1813–1832. https://doi.org/10.1180/minmag.2015.079.7.11.

Wang, M., Gutzmer, J., Michalak, P.P., Guo, X., Xiao, F., Wang, W., Liu, K., 2014. PGE geochemistry of the Fengshan porphyry–skarn Cu–Mo deposit, Hubei Province, Eastern China. Ore Geology Reviews 56, 1–12. https://doi.org/10.1016/j.oregeorev.2013.07.006.

Xiong, Y., Wood, S.A., 2000. Experimental quantification of hydrothermal solubility of platinum-group elements with special reference to porphyry copper environments. Mineral. Petrol. 68, 1–28. https://doi.org/10.1007/s007100050001.

Yano, R.I., 2012. Trace Element Distribution in Chalcopyrite-Bearing Porphyry and Skarn Deposits. Ms.c. Thesis. University of Nevada, Reno (103 pp).

Zarasvandi, A., Rezaei, M., Raith, J.G., Pourkaseb, H., Asadi, S., Saed, M., Lentz, D.R., 2018. Metal endowment reflected in chemical compo- sition of silicates and sulfides of mineralized porphyry copper systems, Urumieh-Dokhtar magmatic arc. Iran: Geochimica et Cosmochimica Acta 223, 36–59.

Zhang, P., Huang, X.-W., Cui, B., Wang, B.-C., Yin, Y.-F., Wang, J.-R., 2016. Re-Os isotopic and trace element compositions of pyrite and origin of the Cretaceous Jinchang porphyry Cu-Au deposit, Heilongjiang Province. NE China. Journal of Asian Earth Sciences 129, 67–80.

Zimmerman, A., Stein, H., Markey, R., Fanger, L., Hein-Rich, C., von Quadt, A., Peytcheva, I., 2003. Re– Os ages for the elatsite Cu–Au deposit, Srednogorie zone, Bulgaria. In: Eliopoulos (Ed.), Mineral Exploration and Sustainable Development. Millpress, Rotterdam, pp. 1253–1256.